Author Manuscript

Author Manuscript

Author Manuscript

Author Manuscript

HHS Public Access

Author manuscript

Cell Rep. Author manuscript; available in PMC 2024 January 03.

Published in final edited form as:

Cell Rep. 2023 October 31; 42(10): 113196. doi:10.1016/j.celrep.2023.113196.

TET3 plays a critical role in white adipose development and diet-induced remodeling

Byung Chul Jung[1], **Dongjoo You**[1], **Ikjun Lee**[1], **Daofeng Li**[2,3], **Rebecca L. Schill**[4], **Katherine Ma**[1], **Anna Pi**[1], **Zehan Song**[1], **Wei-Chieh Mu**[1], **Ting Wang**[2,3], **Ormond A. MacDougald**[4], **Alexander S. Banks**[5], **Sona Kang**[1,6,*]

[1]Nutritional Sciences and Toxicology Department, University of California Berkeley, Berkeley, CA, USA

[2]Department of Genetics, Washington University School of Medicine, St. Louis, MO, USA

[3]The Edison Family Center for Genome Sciences and Systems Biology, Washington University School of Medicine, St. Louis, MO, USA

[4]Department of Molecular & Integrative Physiology, University of Michigan School of Medicine, Ann Arbor, MO, USA

[5]Division of Endocrinology, Diabetes and Metabolism, Beth Israel Deaconess Medical Center and Harvard Medical School, Boston, MA, USA

[6]Lead contact

SUMMARY

Maintaining healthy adipose tissue is crucial for metabolic health, requiring a deeper understanding of adipocyte development and response to high-calorie diets. This study highlights the importance of TET3 during white adipose tissue (WAT) development and expansion. Selective depletion of *Tet3* in adipose precursor cells (APCs) reduces adipogenesis, protects against diet-induced adipose expansion, and enhances whole-body metabolism. Transcriptomic analysis of wild-type and *Tet3* knockout (KO) APCs unveiled TET3 target genes, including Pparg and several genes linked to the extracellular matrix, pivotal for adipogenesis and remodeling. DNA methylation profiling and functional studies underscore the importance of DNA demethylation in gene regulation. Remarkably, targeted DNA demethylation at the *Pparg* promoter restored its transcription. In conclusion, TET3 significantly governs adipogenesis and diet-induced adipose expansion by regulating key target genes in APCs.

This is an open access article under the CC BY-NC-ND license (http://creativecommons.org/licenses/by-nc-nd/4.0/).

*Correspondence: kangs@berkeley.edu.

AUTHOR CONTRIBUTIONS

Conceptualization, S.K.; methodology, B.C.J. and S.K.; software, B.C.J., D.L., W.-C.M., T.W., O.A.M., and A.S.B.; validation, B.C.J., D.Y., and I.L.; investigation, B.C.J., D.Y., I.L., K.M., R.L.S., and A.P.; resources, D.L., R.L.S., Z.S., W.-C.M., T.W., O.A.M., and A.S.B.; writing – main text, S.K.; writing – review & proofreading, B.C.J. and S.K.; visualization, B.C.J. and D.Y.; supervision, S.K.; project administration, S.K.; funding acquisition, S.K.

DECLARATION OF INTERESTS

The authors declare no competing interests.

SUPPLEMENTAL INFORMATION

Supplemental information can be found online at https://doi.org/10.1016/j.celrep.2023.113196.

Author Manuscript
Author Manuscript
Author Manuscript
Author Manuscript

In brief

Jung et al. show that Tet3 plays critical role in white adipose tissue (WAT) development and expansion and that *Tet3* ablation in adipocyte precursor cells leads to reduced adipogenesis and expansion, consequently contributing to improvement of metabolic health.

Graphical Abstract

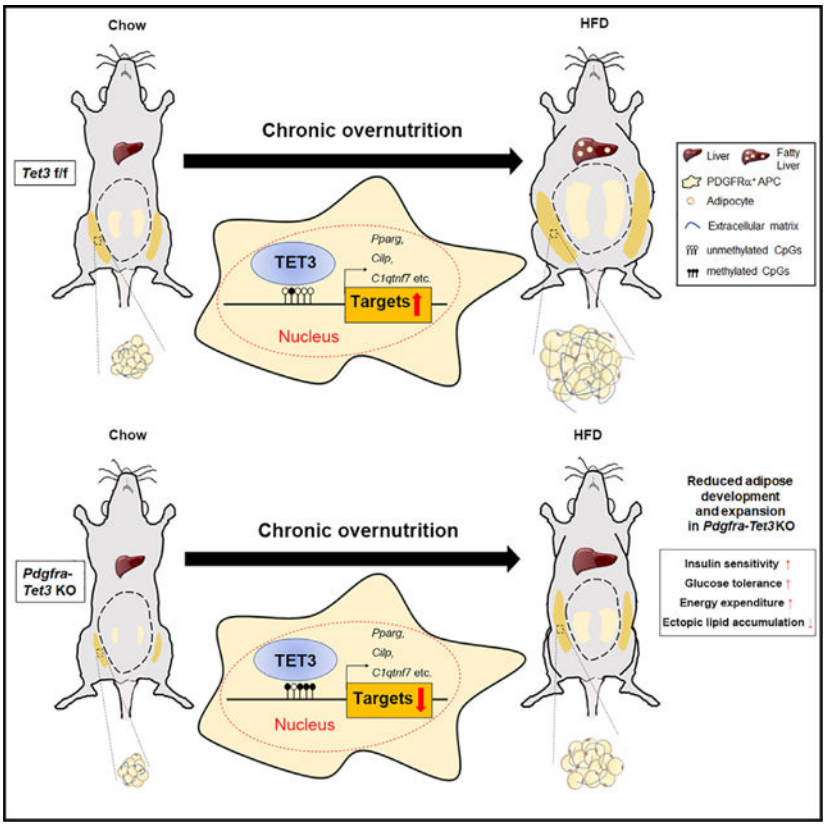

INTRODUCTION

White adipose tissue (WAT) is essential for regulation of energy homeostasis and whole-body metabolism.[1] In particular, adipocytes are responsible for storing fat that is released during energy shortage and for secretion of a number of adipokines.[1] Both excessive and insufficient amounts of WAT are detrimental to the health of an organism, as both states cause ectopic lipid deposition in non-adipose tissues that results in metabolic insults, including insulin resistance and adipose fibro-inflammation.[2–5] Maintaining a moderate amount of healthy WAT is therefore essential for metabolic health, and it is critical to understand mechanisms that control adipocyte developmental and remodeling processes.

Epigenetic changes are modifications to DNA that regulate whether genes are turned on or off. Accumulating evidence indicates that epigenetic factors play important roles in the regulation of adipocyte development and plasticity and that they mediate the interplay between genes and environment.[6–9] DNA methylation is a type of reversible epigenetic

Author Manuscript Author Manuscript Author Manuscript Author Manuscript

modification mediated by DNA methyltransferases (DNMTs) and tends to occur at the 5′ carbon of the cytosine ring (5C), forming 5-methylcytosine (5mC).[10] DNA methylation has long been considered a static epigenetic modification, but emerging evidence suggests that it undergoes dynamic and reversible remodeling.[11] TET proteins (TET1, −2, and −3) are a group of enzymes involved in active DNA demethylation. They act as a 5mC dioxygenase, converting 5mC to 5hmC as the first step of DNA demethylation. TET enzymes can also oxidize 5mC or 5hmC to generate 5-formylcytosine (5fC) and/or 5-carboxylcytosine (5caC).[11]

Our group and others have demonstrated that DNA (de) methylation is involved in multiple aspects of adipose biology.[8,9,12–16] Several studies have reported that key adipocyte genes undergo demethylation during adipogenesis, correlating with increased gene expression. For example, *Pparg* promoter regions have been shown to undergo gradual demethylation during 3T3-L1 adipogenesis.[17] This coincides with other epigenetic changes, such as the loss of repressive histone marks (H3K9me3) and the gain of active marks (e.g., H3K27ac and H3K4me3).[18] Similarly, reduced DNA methylation has been observed at promoters of other key adipocyte genes (e.g., *Cebpa16*, Lep,[19] Slc2a4,[20] and Plin115) during adipogenesis. Global profiling studies showed that 5hmC is enriched at adipocyte-specific enhancers and in PPARγ^{+} nuclei of human adipocytes[21] and that it co-localizes with PPARγ at enhancers in 3T3-L1 adipocytes.[22]

A previous study reported that TET1 and TET2 are necessary for 3T3-L1 adipocyte differentiation.[17] Other *in vitro* studies have found that TET1 and TET2 facilitate expression of key adipocyte genes, such as *Plin1*[15] and *Adipoq*,[12] respectively, by physically interacting with PPARγ. It has therefore been suggested that TET1 and/or TET2 are also critical mediators of DNA demethylation of adipocyte genes during *in vivo* adipogenesis. In contrast, we have found that expression of *Tet3*, rather than *Tet1* or *Tet2*, increases significantly during adipogenesis in naive adipose precursor cells (APCs), as well as in various preadipocyte cell lines.

Here, we explored the role of TET3 in adipogenesis *in vivo* and the metabolic consequences of *Tet3* deficiency. We show that TET3 cell autonomously facilitates adipogenesis. APC-selective *Tet3* knockout (KO) mice on either a chow or high-fat diet displayed a decreased adipose mass with reduced adipogenesis while not manifesting a lipodystrophy phenotype. Strikingly, these KO mice were resistant to diet-induced obesity without metabolic impairment. This metabolic advantage was accompanied by reduced fibro-inflammation in WAT. Our genome-wide profiling reveals that TET3 regulates a set of previously unsuspected target genes in APCs, concurrent with modifications of their DNA methylation profile, which are critical for adipogenesis and adipose remodeling. Finally, we validate the importance of TET3-dependent changes of DNA methylation at TET3 target genes as gene regulatory elements by DNA methylation-dependent reporter assays and site-specific modification of DNA demethylation. Taken together, our studies demonstrate that TET3 is a critical epigenetic regulator of homeostatic control of WAT development and diet-induced adipose expansion.

Author Manuscript Author Manuscript Author Manuscript Author Manuscript

RESULTS

TET3 regulates adipogenesis cell autonomously

Results from our previous research indicate that TET2 and TET3 levels are significantly increased during adipogenesis in 3T3-L1 (considered as white), beige, and brown adipocyte cell lines.[8] To determine whether TETs regulate *in vivo* adipogenesis, and if so, which of them might do so, we investigated TET expression patterns during adipogenesis of primary APCs. APCs were defined by expression of PDGFRα (a commonly chosen APC surface marker[23–26]) in stromal vascular fraction (SVF) cells and by the absence of hematopoietic markers (Lin; CD31, CD45, Ter119) (Figure S1A). Upon isolation of APCs using fluorescence-activated cell sorting (FACS) from lean wild-type (WT) mice, we compared *Tet* expression before and after adipogenesis. The results showed that *Tet3* transcription increased by ~3-fold during APC differentiation; in contrast, *Tet2* transcript levels did not change, whereas *Tet1* transcript rather decreased (Figure S1B). Assessment of a published single-cell RNA sequencing (scRNA-seq) database profiled from mouse WAT[27] revealed an overall positive correlation between *Tet3* and *Pdgfra* transcript expression within *Pdgfra*$^{+}$ APCs (Figure S1C). Additionally, we have conducted the tissue distribution analysis of TET3 expression and found that TET3 expression is detected in various tissues, but it is relatively higher in white adipose depots compared with brown adipose tissue (BAT), liver, and skeletal muscle (Figure S1D). This relationship prompted us to investigate the roles of TET3 in adipogenesis *in vivo*. We generated mouse models of APC-selective *Tet3*-deficient mice by crossing *Tet3*-floxed mice with *Pdgfra*-Cre (Figure 1A), which has been used to target a broad range of APC populations.[23–26] We first confirmed a highly efficient *Tet3* knockdown (KD) of >90% in FACS-purified APCs from inguinal WAT (iWAT) and epididymal WAT (eWAT) of KO and WT mice (Figure 1B). To determine the cell-autonomous role of TET3 in adipogenesis, we then FACS-purified Lin^{-}/PDGFRa^{+} iWAT APCs from 8-week-old WT and KO mice on a chow diet and differentiated them in culture by using the standard differentiation inducers (i.e., dexamethasone, 3-isobutyl-1-methylxanthine (IBMX), insulin). KO APCs showed reduced adipogenic competency, as assessed by oil red O (ORO) staining and gene expression analysis of key adipocyte markers (e.g., *Pparg*, *Fabp4*, *Scd1*, and *Lipe*) (Figures 1C and 1D). To further determine cell-autonomous role of TET3 in adipogenesis, we assessed adipogenic capacity of 3T3-L1 cells upon TET3 overexpression (OE) and *Tet3* KD. First, we confirmed that OE and KD increased and decreased 5hmC levels, respectively (Figures 1E and 1I). When assessed by lipid accumulation and gene expression analysis of adipocyte markers, TET3 OE promoted adipogenesis, while *Tet3* KD impaired differentiation (Figures 1F–1H and 1J–1L). Together, these data indicate a cell-autonomous role for TET3 in facilitating adipogenesis.

TET3 is necessary for WAT development under chow-fed conditions

We next used *Pdgfra-Tet3* KO mice to investigate roles of TET3 in WAT development. When animals were fed a chow diet, no significant difference was found in body weight (BW) between genotypes (Figure 2A). However, *Pdgfra-Tet3* KO mice exhibit significant reductions of 22% and 40% in fat and WAT mass, respectively, in comparison to their littermate controls. This was determined by EchoMRI and measurement of tissue weights (Figures 2B and 2C). Histological examination was then carried out using H&E staining

Author Manuscript Author Manuscript Author Manuscript Author Manuscript

(Figures 2D and 2G) and adipocyte size distribution analysis to assess adipocyte formation and morphology. Overall, we found that adipocyte size did not differ between genotypes (Figures 2E and 2H), but total adipocyte number was overall reduced in iWAT and eWAT of KO mice compared with controls (Figures 2F and 2I). Our gene expression analysis of KO mice showed reduced expression of key adipocyte genes, including *Pparg*, *Scd1*, *Lipe*, and *Lep*, in both iWAT and eWAT depots, and this decrease was particularly pronounced in iWAT (Figures 2J–2M). Importantly, although KO mice had reduced WAT, no differences were observed in their energy expenditure, physical activity, food intake, or respiratory exchange rate (RER) (Figures S2A–S2D). In line with this, no significant change was observed in expression of *Ucp1* in various adipose depots, including iWAT and BAT (Figure S2E). We also did not find discernable differences in BAT histology (Figure S2F). These data suggest that reduced adiposity is not due to increased energy expenditure. Together, these data suggest that TET3 is required for the full complement of adipocytes under chow-fed conditions.

Tet3 deficiency in APCs confers protection from diet-induced unhealthy adipose expansion and remodeling

High-fat feeding induces adipose expansion by promoting *de novo* adipogenesis and hypertrophy.To determine the roles of TET3 in diet-induced adipose tissue expansion, a cohort of male mice were fed a high-fat diet (HFD). Remarkably, KO mice were generally found to gain less weight, weighing significantly less than control mice after 10 weeks of HFD feeding (Figures 3A and 3B). This difference was primarily due to reduced fat mass in KO mice (Figures 3C and 3D). Tissue measurement confirmed that weight of various WAT depots was significantly reduced in KO mice on an HFD compared with control WT litter-mates (Figure 3E). Analyses of adipocyte size distribution indicated that iWAT and eWAT of KO mice were reduced in size (Figures 3F, 3G, 3I, and 3J), as was total adipocyte number (Figures 3H and 3K). Several key adipocyte genes showed reduced expression in both iWAT and eWAT. The reduction was more pronounced in iWAT, similar to that seen in chow-fed mice (Figures 3L–3N). In agreement with reduced adiposity, serum leptin levels were lower in KO mice than in WT mice (Figure 3O). We also determined whether altered energy homeostasis contributed to reduced mass. Compared with control WT mice, KO male mice on an HFD showed higher energy expenditure and had increased resting whole-body energy expenditure when differences in body mass were accounted for by analysis of covariance (ANCOVA) (Figure S3A), while there were no changes in food intake, physical activity, or RER (Figures S3B–S2D). We therefore investigated whether KO mice have increased adipose thermogenesis. We found that *Pdgfra-Tet3* KO mice had increased expression of *Ucp1* in iWAT, but not in eWAT or BAT, compared with controls (Figure S3E). Notably, we observed a significant reduction in BAT weight (Figure 3E) and lipid accumulation in KO mice (Figures S3E and S3F). These data suggest that increased energy expenditure contributes to reduced adiposity in KO animals fed an HFD.

As we observed a reduction in total adipocyte number in KO mice, we then determined whether this was due to altered APC proliferation and/or increased apoptotic rates. To evaluate the levels of apoptosis, we performed terminal deoxynucleotidyl transferase 2′-deoxyuridine-5′-triphosphate (dUTP) nick end labeling (TUNEL) assays, a method based

Author Manuscript Author Manuscript Author Manuscript Author Manuscript

on detection of 5-Bromo-dUTP (Br-dUTP), which are incorporated into fragmented DNA. We observed that the apoptotic rate was generally lower in iWAT KO APCs compared with WT controls, while it remained unchanged in eWAT KO APCs (Figure S4A). No major changes were detected in the expression of pro- and antiapoptotic genes (e.g., *Bax*, *Bak*, *Bcl2*, *Bcl-xL*) between genotypes in both WAT depots (Figures S4B and S4C). These results suggest that the lower adipocyte number was not due to loss of APC pools. Next, APC proliferation was measured by using BrdU, a base analog of thymidine that is incorporated into DNA in place of thymidine, providing a measurement of DNA synthesis and cell proliferation. To examine diet-induced APC proliferation, we fed a cohort of chow-fed mice BrdU-containing water (0.8 mg/kg) for 1 week at 8 weeks of age and put them on an HFD. Following BrdU administration, fractionated SVF cells were stained with surface antibodies for Lin markers and PDGFRα. Cells were then fixed and permeabilized for staining with BrdU antibodies. Our results identified no discernable changes in APC proliferation between genotypes (Figure S4D), suggesting that the reduced *de novo* adipogenesis observed in KO mice was not due to compromised APC proliferation.

Diet-induced adipose remodeling involves increased inflammation and fibrosis, signifying adipose tissue dysfunction.[2,28,29] Our experiments showed reduced macrophage infiltration in KO WAT, as indicated by a lower number of crown-like structures (Figures 3F and 3I) and fewer cells stained with Mac2 (a surface macrophage marker) (Figure 3P). In addition, we noted that KO WAT demonstrated reduced expression of inflammatory cytokines and fibrosis markers (Figures 3L and 3M) and had lower quantities of hydroxyproline (a major component of fibrillar collagen) (Figure 3Q).

In both humans and mice, 50%–70% of the bone marrow cavity is filled with bone marrow adipocytes,[30] which likely play a role in local bone homeostasis. Since PDFGRa is expressed in mesenchymal cells in the bone marrow, we sought to investigate whether the Tet3 deficiency in mice PDFGRα$^+$ cells has an impact on bone parameters. To do that, we performed microcomputed tomography (μCT) imaging of the tibiae bones of WT and *Pdgfra-Tet3* KO mice and detected no discernible changes in tibiae bone parameters between genotypes in both genders on either diet (Figure S5). Taken together, our data indicate that Tet3 deficiency in APCs results in protection from unhealthy diet-induced adipose expansion and remodeling.

APC-selective *Tet3* deficiency improves metabolic health in mice upon chronic high-fat feeding

We investigated the metabolic consequences of reduced adipogenesis caused by APC-selective Tet3 deficiency. No significant differences in metabolic profile were observed between WT and *Pdgfra-Tet3* KO male mice on a chow diet, including their glucose tolerance and insulin sensitivity, as assessed by glucose and insulin tolerance tests (GTTs and ITTs, respectively) (Figures 4A–4D). We then fed a cohort of WT and KO male mice an HFD starting at 8 weeks of age to determine whether this would affect the metabolic profile. Remarkably, after 6–7 weeks of HFD feeding, KO male mice exhibited improved glucose tolerance and demonstrated hypoglycemia during fasting as well as during GTTs and ITTs (Figures 4E, 4F, and 4G). KO male mice also showed a reduced level of homeostatic

Author Manuscript Author Manuscript Author Manuscript Author Manuscript

model assessment for insulin resistance (HOMA-IR), but there was no significant difference observed in the kinetics of glucose clearance following insulin injection (Figures 4G–4I). Sex-specific differences have been reported in several aspects of adipose biology, including development and responses to metabolic adaptation.[31–33] Therefore, we examined a cohort of female mice to determine whether TET3 acts in the same manner as a male cohort in this biological context. Our results showed that KO female mice had generally reduced fat mass (Figures S6A–S6C) and improved glucose tolerance following prolonged feeding on an HFD (Figures S6D–S6G), although the extent of these effects was somewhat less pronounced than in the male cohort. We conclude that it is likely that the role of TET3 is largely conserved in both male and female mice. Next, we determined the impact of reduced adiposity in *Pdgfra-Tet3* KO mice on hepatic lipid accumulation. On a chow diet, we did not observe ectopic lipid accumulation in the liver of *Pdgfra-Tet3* KO male mice (Figure 4J). In contrast, when on an HFD, KO male mice showed a dramatic reduction of hepatic triglyceride (TG) accumulation (Figures 4J and 4K), which indicates that APC-specific *Tet3* deficiency does not cause lipodystrophy but does confer protection from diet-induced metabolic impairment of hepatosteatosis.

TET3 regulates adipogenesis through key target genes in APCs, particularly extracellular matrix (ECM)-related genes

We and others have demonstrated that TETs control many biological processes by regulating sets of specific target genes.[8,12,34] To reveal the underlying molecular mechanisms by which TET3 regulates adipogenesis, we performed genome-wide RNA-seq and DNA methylation profiling studies, comparing WT and KO APCs from mice fed an HFD (Figure 5A). By transcriptomic analysis, we identified 176 and 153 genes that were up- and downregulated in KO APCs, respectively (Figure 5B; Table S1). As TET3 mediates DNA demethylation, we hypothesized that loss of *Tet3* would lead to DNA hypermethylation of target genes, resulting in gene repression. We therefore focused our attention on the downregulated genes, which were most likely to be the direct targets of TET3. Pathway analysis indicated that several biological pathways involved in ECM remodeling were highly enriched in the downregulated gene sets (e.g., *Cilp*, *C1qtnf7*, *Col8a1*, *Mgp*) (Figures 5C and 5D). Although it was just under the threshold of significance in the RNA-seq analysis, our qPCR analysis identified *Pparg* as a downregulated gene in *Tet3* KO APCs (Figure 5D). While we observed pathways enriched in upregulated gene sets, we have not found them to be relevant in the *Tet3* KD phenotypes we have observed thus far (Figure S7). In addition, these enriched pathways were less statistically significant when compared with the enriched pathways found in the downregulated gene sets.

Excessive ECM production has been linked to unhealthy adipose formation and insulin resistance,[35] though mechanisms underlying these processes are not well understood. Of the ECM-related TET3 target genes, we chose to prioritize to study *Cilp*, as it demonstrated a cell-autonomous downregulation with *Tet3* KD in 3T3-L1 preadipocytes (Figure 5E), increased expression during adipogenesis (Figure 5F), and elevated expression in obese WAT (Figure 5G), with hypermethylated CpGs at the gene locus (Figure 6F). *Cilp* encodes the cartilage intermediate layer protein (CILP), a matricellular protein produced by chondrocytes in articular cartilage,[36] and CILP has been implicated in

Author Manuscript Author Manuscript Author Manuscript Author Manuscript

common musculoskeletal disorders, including osteoarthritis and lumbar disc degeneration.[37] It has also been associated with cardiac ECM remodeling in mouse hearts undergoing pathological ventricular remodeling, such as during myocardial infarction and transverse aortic constriction.[38–40] Notably, recent scRNA-seq studies identified *Cilp* as one of the extracellular markers enriched in specific subpopulations of APCs.[41,42] Despite its relevant implications, the role of CILP in regulating adipogenesis and adipocyte remodeling has not yet been investigated. Thus, we sought to determine the functional importance of CILP in TET3-mediated adipogenesis by gain-of-function studies. Remarkably, 3T3-L1 cells treated with recombinant CILP had enhanced adipogenic capacity, as assessed by ORO and gene expression analysis (Figures 5H and 5I). Our data suggest that CILP may be a critical molecular target for TET3 in promoting adipogenesis.

TET3-dependent modification of DNA methylation in APCs is critical for target gene regulation and adipogenesis

TETs have been shown to mediate biological processes through DNA-demethylase-dependent and -independent regulation of target genes, depending on the biological context.[43] We therefore investigated whether the catalytic activity of TET3 is essential for regulating adipogenesis. We first performed gain-of-function studies using various TET3 alleles in 3T3-L1 cells: TET3-WT (full-length WT), TET3-CD (catalytic domain only),[44] and TET3-CDM (full length with catalytic-dead mutation)[44] (Figure S8A). When these alleles were overexpressed to a similar degree, OE of TET3-WT and TET3-CD enhanced adipogenesis, whereas OE of TET3-CDM did not (Figures S8B and S8C). Additionally, we conducted a rescue experiment by reintroducing an equivalent amount of TET3-WT vs. TET3-CDM allele in *Tet3* KD cells (Figures S8D and S8E). Our results showed that only the WT allele significantly restored diminished adipogenesis in *Tet3* KD cells (Figures S8E and S8F). Together, these data demonstrate that DNA demethylase activity of TET3 is required for its effect on adipogenesis.

Next, to determine the epigenetic basis of TET3 regulation of target genes, we profiled DNA methylomes of naive WT and KO APCs from mice fed an HFD using whole-genome bisulfite sequencing (WGBS), a gold-standard method of measuring DNA methylation profiles at bp resolution.[45] We defined differentially methylated regions (DMRs) as at least 5 CpGs in 200 bp bins, with minimal differences in methylation level (>20%, $p < 0.01$). Consistent with the theory that TET3 mediates DNA demethylation, genome-wide *Tet3* KO APCs showed a much higher number of hypermethylated DMRs (hyper-DMRs; n = 1811) than hypomethylated DMRs (hypo-DMRs; n = 9) (Figures 6A and 6B). We found that 32.7% (50/153) of downregulated genes in KO APCs were associated with hyper-DMRs within a 50 kb distance of transcription start sites (Figure 6C). To identify relevant biological pathways associated with methylation changes resulting from *Tet3* deficiency, we performed pathway analysis of genes linked to hyper-DMRs in KO APCs. Remarkably, several Kyoto Encyclopedia of Genes and Genomes (KEGG) pathways involved in cell remodeling were found to be enriched (Figure 6D), which were consistent with genes downregulated in KO APCs (Figures 5B–5D). Hypermethylation was observed at the *Pparg* (Figure 6E) and ECM-related genes, such as *Cilp* and *C1qtnf7* (Figures 6F and 6G), and we therefore sought to determine the importance of DNA methylation of hyper-DMRs in gene regulation. We

Author Manuscript Author Manuscript Author Manuscript Author Manuscript

subcloned the target hyper-DMRs near TET3 target genes (i.e., *Pparg*, *Cilp*, and *C1qtnf7*) to a DNA-methylation-dependent reporter plasmid (pCpGL-Basic) that lacked backbone CpG dinucleotides.[46] Our results showed that methylase treatment significantly reduced reporter activities of the pCpGL-containing hyper-DMRs of *Pparg*, *Cilp*, and *C1qtnf7* by ~40%–70%, but no effect was found on the pCpGL itself or the vector containing the CpG-free gene activation element (pCpGL-CMV/EF1) (Figure 6H). Furthermore, our TET3 chromatin immunoprecipitation (ChIP) analysis confirmed that TET3 binds to these hypermethylated regions in *Tet3* KO APCs (Figures 6I–6K). Together, these data indicate that TET3 regulates expression of target genes by modifying their DNA methylation profiles.

TETs are known to be recruited to DNA by sequence-specific transcription factors in different biological contexts.[34,47,48] We therefore queried the DNA sequence of hyper-DMRs in KO APCs to predict the candidate factor(s) that confers TET3 target specificity. Most notably, motif analysis of hyper-DMRs showed high enrichment for the transcription factors known to be important in adipogenesis (Figure 6L). For example, the nuclear factor I (NFI) transcription factors have previously been shown to be pro-adipogenic in multiple adipogenesis models.[49–51] The CCAAT-enhancer-binding protein (CEBP) family of transcription factors are also well recognized for their critical role in initiating and enhancing adipogenesis.[52] Of note, C/EBPβ and -δ have been shown to orchestrate chromatin remodeling in 3T3-L1 adipogenesis.[53,54] It was interesting to note that the CEBPε motif ranked highly as an enriched at hyper-DMRs in KO, although it was not the most highly expressed CEBP transcription factor in adipocytes. This could be due to the inaccuracy of motif prediction in distinguishing different gene family members.

CRISPR-dCas9-mediated DNA hydroxymethylation at the *Pparg* promoter is sufficient to increase its expression

PPARγ is a master transcription factor of adipogenesis. It has two main isoforms—γ1 and γ2— that are generated from separate transcriptional start sites, resulting in 30 additional amino acids at the PPARγ2 N terminus.[55,56] We found that expression of both isoforms of PPARγ was reduced in KO WATs. In particular, our data indicate that TET3 regulates expression of *Pparg2* by modifying methylation levels of the promoter region (Figures 6E, 6H, and 6I). Thus, we attempted to introduce DNA hydroxymethylation at the *Pparg2* promoter region to determine whether this would be sufficient to alter *Pparg2* gene expression. To do that, we used CRISPR-dCas9-based approaches with endogenous *cis*-regulatory elements that allow target specificity. A chimeric DNA demethylase tool was developed by fusing the TET1 catalytic domain to the nuclease-dead double Cas9 in a doxycycline-inducible lentivirus (pINDUCER-dCas9-TET1CD).[57] A catalytic mutant version of this (pINDUCER-dCas9TET1CDM)[57] was used as a control. To target the *Pparg* hyper-DMR, we tested 3 gRNAs subcloned into a lentiviral gRNA expression vector (pLN-U6-gRNA). 3T3-L1 cells underwent lentiviral transduction, producing pINDUCER-dCas9-TET1CD or pINDUCER-dCas9-TET1CDM. These cells reliably expressed the fusion proteins and were then transduced with pLN-U6-*gPparg* and control gRNAs. We found that pINDUCER-dCas9-TET1CD cells co-expressing *Pparg* gRNA (particularly #2 gPparg2) increased *Pparg* expression by approximately 7-fold following doxycycline administration, while there was a marginal increase in pINDUCER-dCas9-TET1CDM cells

Author Manuscript Author Manuscript Author Manuscript Author Manuscript

(Figure 6M). Our methylated DNA immunoprecipitation (MeDIP) analysis confirmed that DNA methylation was successfully reduced at the targeted region in pINDUCER-dCas9-TET1CD cells (Figure 6N). Next, to test whether targeted DNA demethylation is sufficient to alter adipogenic capacity, we transduced control and *shTet3* KD 3T3-L1 cells with *gPparg* (#2) and pINDUCER-dCas9-TET1CD. We found that *gPparg*-expressing cells showed a significant increase in adipogenic gene expression in both control and *shTet3* KD cells (Figure 6O). These results indicate that the DNA methylation level of the *Pparg2* promoter is critical for modulation of *Pparg2* expression and adipogenesis.

DISCUSSION

Adipocyte formation and diet-induced adipose expansion involve dramatic changes in epigenetic modifications. Here, we demonstrate that TET3 is a critical epigenetic regulator of *in vivo* adipogenesis by employing *Pdgfra-Tet3* KO mice with APC-selective targeting. Our data also show that, rather than causing lipodystrophy, the reduced adipogenesis observed in KO mice is associated with protection from diet-induced obesity and improves whole-body metabolism when mice are challenged with an HFD. Genome-wide transcriptomic and epigenomic profiling studies (followed by functional validation studies) on naive WT and *Tet3* KO APCs revealed a set of previously unsuspected TET3 molecular and genomic targets. Furthermore, we successfully induced DNA demethylation at the *Pparg* promoter region using a programmable CRISPR-dCas9-based demethylase tool and were thus able to alter the expression of *Pparg*.

While preparing our manuscript, we learned of a highly relevant paper recently published by Park et al.[53] These authors reported that TET3-mediated DNA demethylation is an essential epigenetic remodeling process for adipogenesis *in vitro* and by plasmid injection into WAT.[53] There appear to be some similarities between our study and that of Park et al.[53] Both studies show that TET3, rather than TET1 or TET2, is critical for adipogenesis. However, this also has been supported by one of our previous studies, which showed that APC-selective *Tet1 KO Pdgfra*-Cre mice did not significantly differ phenotypically in adipose development or whole-body metabolism.[8] We also did not observe significant phenotypic changes in adiposity in whole-body *Tet2* KO mice (data not shown). It should be noted, however, that our current results show critical points absent in Park et al.[53] We generated and used conditional KO mice to achieve APC-selective *Tet3* deficiency, thus demonstrating the pro-adipogenic role of TET3 and metabolic consequence logologically. Moreover, we performed WGBS analysis in parallel with transcriptomic analysis of naive WT and *Tet3* KO APCs, which enabled us to identify the epigenetic and transcriptional targets of TET3. We also provide evidence supporting the functional importance of TET3 target genes and target CpGs. In this regard, Park et al.[53] performed WGBS analysis using a 3T3-L1 cell model to detect selectively reduced DNA methylation at genes induced during adipocyte differentiation. Interestingly, our motif analysis at the hyper-DMRs in *Tet3* KO APCs predicted the involvement of several transcription factors for TET3-mediated adipogenesis, including NFIX and C/EBPε. The motifs for these two transcription factors were also found to be enriched in the hypo-DMRs of promoters and enhancers induced during 3T3-L1 adipogenesis.[53]

Author Manuscript Author Manuscript Author Manuscript Author Manuscript

In addition to identifying roles of TET3 in adipogenesis *in vivo*, our *Pdgfra-Tet3* KO mice allowed us to address metabolic consequences of APC-selective *Tet3* deficiency. Severe defects in adipogenesis often result in lipodystrophy, as observed in adipocyte-specific *Pparg* KO[4,5] and A-ZIP/F[58] mice. These models, along with other lipoatrophic mouse models,[59–61] exhibit the typical metabolic sequelae of lipodystrophy, including ectopic lipid accumulation, hyperglycemia, hyperinsulinemia, and severe insulin resistance. However, in the case of *Tet3*-deficient APCs, we observed a reduction in adipogenesis rather than complete loss. As a result, *Pdgfra-Tet3* KO mice did not display a phenotype indicative of adipose tissue insufficiency phenotype. In fact, these mice exhibited a metabolic advantage when subjected to chronic HFD feeding. We propose that this phenomenon is partly attributed to the moderate reduction of PPARγ in WAT caused by *Tet3* deficiency. Remarkably, similar metabolic improvement has been reported in mouse genetic models with partial loss of *Pparg* function.[62,63]

For example, studies have shown that mice lacking a single copy of *Pparg* are protected from diet-induced obesity and glucose intolerance,[62] suggesting that *Pparg* produces a dose-dependent effect. Most recently, a study generating *Pparg* iso-form-specific KO mice showed that both *Pparg1* and *g2* KO mice demonstrate resistance to diet-induced obesity and have higher glucose tolerance.[63] Likewise, our results showing improved organismal metabolism in *Pdgfra-Tet3* KO mice fed an HFD are consistent with the reduced *Pparg* expression levels observed in several previous mouse genetic models.[62,63] Taken together, the findings of these studies suggest that reducing PPARγ expression or activity results in protection from diet-induced obesity and metabolic dysregulation rather than lipodystrophy. As such, the identification of *Pparg* as a direct target gene of TET3 and the potential to alter *Pparg* expression with site-specific DNA demethylation are highly notable findings in the context of developing therapeutic interventions for metabolic diseases.

WAT ECM remodeling is essential for various biological activities in adipose tissue, including effective adipogenesis,[64] tissue architecture,[65] and intercellular interactions in the tissue niche.[66] Studies have shown that excessive accumulation of ECM components and subsequent interstitial deposition of fibrotic material observed in obesity worsens fibrosis, inflammation, and metabolic impairment.[35,67–69] Collagens are major constituents of adipose tissue ECM. They are primarily produced by adipocytes but also other cell types, including preadipocytes and stem cells.[70] Accumulation of various collagens has been observed in obesity; for example, studies in humans reported that collagen VI expression is positively correlated with body mass index, insulin resistance, and hyperglycemia and that it is associated with increased expression of inflammatory genes.[71] Collagen VI KO has also been shown to improve adipocyte survival and enhance whole-body metabolism.[72] Metalloproteinases (MMPs) are proteases that remodel ECM proteins through cleavage. MMP14, for example, has been identified as required for proper adipogenesis *in vitro* and *in vivo*. Some MMPs (MMP3, −11, −12, −13, −14) have been shown to be upregulated in obesity, while others (MMP7, −9, −16, and −24) are downregulated.[73] In our investigations, we observed that transcripts of several collagen (e.g., *Col4a1*, *Col4a2*, *Col5a2*, *Col5a3*, *Col6a1*, *Col6a3*, *Col6a5*, *Col15a1*, *Col8a1*) and MMP (*Mmp3* and *Mmp11*) genes were downregulated in KO APCs. We therefore suggest that reduced ECM deposition could be a contributing factor in the reduced fibro-inflammation and metabolic improvement

Author Manuscript Author Manuscript Author Manuscript Author Manuscript

observed in *Pdgfra-Tet3* KO mice. Of the ECM-related TET3 target genes, *Cilp* was of particular interest to us, as it has been shown to be involved in pathogenic ECM remodeling in common musculoskeletal disorders[36] and several cardiac diseases.[37] Interestingly, we also found that *Cilp* is highly induced during adipogenesis and in obesity. We therefore investigated the role of *Cilp* in adipogenesis and found that CILP gain of function promotes adipogenesis in vitro. Addressing the function of CILP *in vivo* is essential, as adipose tissue remodeling involves intricate interactions with other cell types in the niche. Given its role as a secretary protein, it will be interesting to determine whether CILP affects the metabolic function of adipocytes in a paracrine manner. Adipose remodeling involves interactions between several different cell types in multiple biological contexts, including angiogenesis, inflammation, and fibrosis. Single-cell resolution studies of entire WAT depots from WT and KO tissues will therefore be helpful to better understand the role of TET3 in adipose tissue remodeling.

In summary, our current study demonstrates a physiological role for TET3 as a critical epigenetic regulator of adipogenesis and diet-induced adipose remodeling. Our genome-wide transcriptional and epigenetic profiling studies, combined with follow-up functional validation studies, have revealed underlying molecular and epigenetic mechanisms by which TET3 regulates these processes.

Limitations of the study

We have observed that approximately two-thirds of hyper-DMRs do not exhibit a correlation with downregulated genes in *Tet3* APCs. This suggests that these specific DMRs, lacking any associations with genes, might have emerged as secondary consequences of the loss of *Tet3*. To discern the direct targets of TET3, further investigations involving TET3 ChIP-seq studies in APCs will be required.

STAR★METHODS

RESOURCE AVAILABILITY

Lead contact—Further information and requests for resources and reagents should be directed to and will be fulfilled by the lead contact, Sona Kang (kangs@berkeley.edu).

Materials availability—Unique reagents generated in this study are available from the lead contact, Sona Kang (kangs@berkeley.edu).

Data and code availability

- The sequencing data reported here has been deposited in NCBI Gene Expression Omnibus and is accessible through GEO: GSE214483.
- This study does not report original code.
- Any additional information required to reanalyze the data reported in this paper is available from the lead contact upon request.

Author Manuscript Author Manuscript Author Manuscript Author Manuscript

EXPERIMENTAL MODEL AND SUBJECT DETAILS

Animal studies—Animal Care Mice were maintained under a 12-h light/12-h dark cycle at constant temperature (23°C) with free access to food and water. All animal work was approved by UC Berkeley ACUC.

Tet3 f/f mice[85] were obtained from Dr. Anjana Rao and *Pdgfra*-Cre was purchased from Jackson Laboratory (#013148). These animals were maintained on a C57BL/6J background. High fat diet (Research Diets, D12331i) was started at 8 week old for 8–12 weeks. For ITT, mice were fasted for 6 h and were i.p. injected with insulin (0.5 U/kg for a chow diet and 0.8 U/kg for HFD cohort). Blood glucose was measured at 0, 15, 30, 60, 90, and 120 min. For GTT, mice were fasted for 6 h and i.p. injected with glucose (1 g/kg for chow and 1.5 g/kg for HFD cohort). Blood glucose levels were measured at 0, 15, 30, 60, and 120 min, using Contour NEXT glucometer and glucose strips.

To calculate the area of the curve (AOC), we subtract the area under the baseline value for a more accurate measure of glucose tolerance and insulin sensitivity, independent of differences in baseline glucose levels.[86] If post-baseline values are lower than the baseline value, the area above the baseline value is considered as the AOC.[87] Metabolic rate was measured by indirect calorimetry in open-circuit Oxymax chambers, a component of the Comprehensive Laboratory Animal Monitoring System (CLAMS; Columbus Instruments). Mice were housed individually and maintained at 25°C under a 12 h light/12 h dark cycle. Activity was monitored in 1 min intervals of infrared beam breaks on the X, Y and z axis and found not to be significantly different for any of the groups. Food and water were available ad *libitum*.

Cell culture—3T3-L1 preadipocytes were obtained from ATCC and these cells were authenticated by the ability to differentiate and confirmed to be mycoplasma negative. The cells were maintained in DMEM supplemented with 10% fetal calf serum and 100 U/ml penicillin, and 100 μg/mL streptomycin. For differentiation, cells at post 2 day confluence were switched to DMEM with 10% fetal bovine serum and exposed to a full (250 μM IBMX, 5 μg/mL insulin, and 1μM dexamethasone) or sub-optimal induction cocktail (0.4x strength of the full cocktail) from day 0–2, insulin from day 2–4, and switch to DMEM with FBS only. For the *ex vivo* culture studies, WAT pads were excised, minced, and digested in PBS containing 2 mg/mL Collagenase type II, 10 mM $CaCl_2$ and 3% bovine serum albumin for 30 min in a shaking water bath at 37°C. Digested fat pads were filtered through 100 μm strainer, followed by centrifugation at 300*g* for 5 min. Pellet is acquired and incubated with RBC lysis buffer for 5 min at RT. Then, cells are filtered through 40 μm strainer and centrifuged at 500*g* for 5 min. After washing with 3% BSA/PBS solution, acquired SVFs were stained with surface antibodies for Lin markers (CD31, CD45, and TER119) and PDGFRα. FACS-purified $Lin^-/PDGFR\alpha^+$ APCs were cultured in DMEM with 10% FBS and differentiated as described above. To generate lentivirus particles, lentiviral constructs were co-transfected with pMD2.G- and psPAX2-expressing plasmids into 293T cells. After 48 h, virus-containing supernatant was collected, filtered through 0.45 μm filters, and added to mature 3T3-L1 adipocytes for 24 h along with 8 μg/mL Polybrene.

Author Manuscript Author Manuscript Author Manuscript Author Manuscript

Transduction efficiency was determined by comparing to cells transduced in parallel with a GFP-expressing lentivirus.

METHOD DETAILS

Protein analysis—Cell or tissue culture samples were lysed in RIPA lysis buffer containing 50 mmol/L Tris-HCl (pH 7.5), 150 mmol/L NaCl, 1% Triton X-100, 0.1% SDS, and protease inhibitor cocktail (Complete Mini-EDTA free, 11836170001, Roche) for 30 min on ice with rotating samples. Protein concentration was quantified by Bradford analysis. 40–60 μg proteins were used for the assays. Proteins were size fractionated by SDS-PAGE and then transferred to polyvinylidene difluoride or nitrocellulose membrane. After blocking with 5% nonfat dried milk in TBS-Tween (0.25%), the membranes were incubated overnight with the appropriate primary antibodies, followed by secondary antibody incubation for 1 h at room temperature. After washing with TBS-Tween for 30 min, signals were detected using the ECL Assay Kit (NEL104001EA; PerkinElmer) using an iBright CL1500 Imaging System (Invitrogen), and quantified with ImageJ.

Reagents—Insulin, dexamethasone, isobutylmethylxanthine (IBMX), puromycin, and Oil Red O were purchased from Sigma. Methylene blue was purchased from Ricca Chemical. Collagenase type 2 was purchased from Fisher scientific. Recombinant CILP protein was purchased from Abcam (182802). Antibodies were purchased from Cell Signaling (HSP-90, 4874; GAPDH, 2118; Mouse (G3A1) mAb IgG1, 5415), Sigma (anti-FLAG, F3165), BD Biosciences (anti-CD45-APC, 561018; CD31-APC, 561814; TER119-APC, 561033), Abcam (5mc, ab10805), Active Motif (5hmc, 39769), Santa Cruz (PPARγ, sc-7273), Cedarlane Labs (MAC-2, CL8942AP) and Millipore (TET3, abe383).

RNA extraction and qPCR—Total RNA was extracted from tissues using TRIzol reagent according to the manufacturer's instructions. cDNA was reverse transcribed from 1 μg of RNA using the cDNA High-Capacity cDNA Reverse Transcription Kit (Applied Biosystems). Quantitative PCR (qPCR) was performed with SYBR green qPCR master mix (AccuPower 2X, Bioneer) using QuantStudio 5 (Applied Biosystems). The relative amount of mRNA normalized to cyclophilin B was calculated using the delta–delta method. Primer sequences are listed in Table S2.

Plasmids—Lentiviral overexpression vectors for TET3-WT, TET3-CD, and TET3-CDM were subcloned into pCDH-CMV-MCS-EF1 vector, and hairpins targeting *Tet3* were subcloned at AgeI/EcoRI to pLKO.1 vector. gRNA to target *Pparg* promoter was cloned at AarI site to pLN-U6-gRNA. Hairpin and gRNA sequences are shown in Table S2 pMD2.G and psPAX2 were gifts from Didier Trono (Addgene plasmid # 12259, #12260; http://n2t.net/addgene:12259, 12260; RRID: Addgene_12259, 12260). pLKO.1 - TRC cloning vector[74] was a gift from David Root (Addgene plasmid # 10878; http://n2t.net/addgene:10878; RRID: Addgene_10878)

ELISA—For the leptin ELISA, serum leptin was analyzed using mouse leptin ELISA Kit (catalog #90030; Crystal Chem). For the insulin ELISA assay, mice were fasted for 6 h. Plasma insulin was analyzed using an ultrasensitive mouse Insulin ELISA kit

Author Manuscript Author Manuscript Author Manuscript Author Manuscript

(#90080; Crystal Chem). The endpoint calorimetric assays were performed using a Plate Reader SpectraMax i3. HOMA-IR was calculated by using homeostasis model assessment-2 (HOMA2) index using an online-based calculator.[88]

Methylation-dependent reporter assay—The CpG-free luciferase reporter vector, pCpGL3-Basic was a kindly gift from Dr. Michael Rehli of University Hospital Regensburg. Target genomic sites were amplified using genomic DNA from C57BL/6J mice and inserted to pCpGL3-Basic vector precut with HindIII/BglII for *Pparg* and BamHI/NcoI for *Cilp* and *C1qtnf7*. Plasmid methylation was carried out using CpG methyltransferase, M.SssI (New England Biolabs) following to the manufacturer's protocol. Briefly, 4 μg plasmids were co-incubated with 160 μM S-sdenosylmethionine (SAM), Sss I (12 U) for 8 h at 37°C. Additional 160 μM SAM was added, and incubated for 16 h. The unmethylated plasmids were prepared as described above, but without adding SAM in the reaction. Purified plasmids were quantified and transiently co-transfected in HEK-293T with Renilla using Lipofectamine 3000 reagent (Invitrogen), following the manufacturer's protocol. After 24 h after transfection, cells were lysed to measure Firefly and Renilla luciferase activity using the Dual-Luciferase Reporter Assay System (Promega). SpectraMax i3 plate reader (Molecular Devices, San Jose, USA) was used to analyze luminescence, and Firefly activity was normalized to Renilla activity.

Dot blotting, ChIP-qPCR, and MeDIP assays—For dot blotting, genomic DNA was extracted using the DNeasy Blood & Tissue kit (Qiagen, 69504) following the manufacturer's protocol. DNA was denatured at 95°C for 15 min in 0.1 M NaOH. It was neutralized with 1 M NH4OAc on ice and diluted to 300 mg in DNase free water. 200 ng DNA was applied to a positively charged nylon membrane under vacuum with a Dot Blot Microfiltration Apparatus (Bio-Rad). The membranes were briefly washed in 2× SSC buffer (0.3 M NaCl, 30 mM sodium citrate) for 5 min, then baked at 80°C for 5 min, and then cross-linked using a UV Stratalinker 1800. Membranes were blocked with 5% nonfat dried milk in TBS-Tween (0.25%). The membranes were incubated with the 5hmC primary antibodies. For a loading control, membranes were stained with methylene blue. Immunoblots were quantified by the ImageJ program. For ChIP-qPCR, cells were cross-linked with 1% formaldehyde for 10 min at room temperature. Cross-linked chromatin was sonicated using an S220 Ultrasonicator (Covaris) to generate DNA fragments of ~200–500 bp. Inputs were taken from cleared lysates, and the rest were rotated O/N at 4°C with TET3 and IgG antibodies for immunoprecipitation. An aliquot of 20 μL of pre-washed Dynabeads Protein G was added per IP and rotated 1 h at 4°C. Beads were successively washed in low-salt RIPA buffer (20 mM Tris-HCl [pH 8.0], 1 mM EDTA, 1% Triton X-100, 0.1% SDS, 140 mM NaCl, 0.1% Na deoxycholate), high-salt RIPA buffer (20 mM Tris-HCl [pH 8.0], 1 mM EDTA, 1% Triton X-100, 0.1% SDS, 500 mM NaCl, 0.1% Na deoxycholate), LiCl buffer (250 mM LiCl, 0.5% NP40, 0.5% Na deoxycholate, 1 mM EDTA, 10 mM Tris-HCl [pH 8.0]) and TE buffer (10 mM Tris-HCl [pH 8.0] and 1 mM EDTA). Each reaction was then incubated in digestion buffer (50 mM Tris-HCl [pH 8.0], 1 mM EDTA, 100 mM NaCl, 0.5% SDS, proteinase K) for a minimum of 4 h at 65°C to reverse cross-links. DNA was recovered using a phenol-chloroform extraction. Real-time qPCR primers are listed in Table S2. All data were normalized to input. For MeDIP, genomic DNA was sheared using a Covaris S220

Author Manuscript Author Manuscript Author Manuscript Author Manuscript

to an average of 200–800 bp. Two micrograms of denatured DNA were incubated with 2 μg of anti-IgG or 5mC antibody in IP buffer (10 mM Na-Phosphate pH 7.0, 0.14 M NaCl, 0.05% Triton X-100) for 2 h at 4°C. Antibody-bound DNA was collected with 20 μL of Dynabeads anti-mouse IgG (Invitrogen Dynal AS) for 1 h at 4°C on a rotating wheel and successively washed five times with washing buffer (0.1% SDS, 1 Triton X-100, 2 mM EDTA, 20 mM Tris-HCI pH 8.1, 150 mM NaCl) and twice with TE (10 mM TrisCl, 1 mM EDTA pH 8.0). DNA was recovered in 125 μL of digestion buffer (50 mM Tris pH 8.0, 10 mM EDTA, 0.5% SDS, 35 mg proteinase K) and incubated for 3 h at 65°C. Recovered DNA was used for qPCR analysis. Primers for MeDIP-qPCR studies are listed in Table S2. All data were normalized to input.

TUNEL assay—Apoptosis rate was measured by using the APO-BrdU Fragmentation Assay Kit (BioVision, K401), which detects the DNA fragmentation of apoptotic cells by exploiting the fact that the DNA breaks expose a large number of 3′-hydroxyl ends. These hydroxyl groups can then serve as starting points for terminal deoxynucleotidyl transferase (TdT), which adds deoxyribonucleotides in a template-independent fashion. Addition of the deoxythymidine analog 5-bromo-2′-deoxyuridine 5′-triphosphate (BrdUTP) to the TdT reaction serves to label the break sites, which can be detected by BrdU antibody. In brief, the SVFs were stained with surface antibodies for Lin markers (CD31, CD45, and TER119) and PDGFRα, followed by fixation with 3.6% Formaldehyde (v/v) for 15 min and ice-cold 70% (v/v) ethanol for 30 min on ice. The fixed cells were incubated with DNA labeling solutions, stained with anti-BrdU-FITC, and incubated with DAPI for 30 min at RT. After washing, resuspended cells were analyzed for BrdU positive cells by flow cytometry (BD LSR Fortessa). Cells that were not incubated with antibody were used as a negative control to determine background fluorescence levels and BrdU positive area was set based on the signals from positive control cells provided in the kit.

Cell proliferation assay—To assess cell proliferation *in vivo*, BrdU was administered in the drinking water at 0.8 mg/mL to incorporate into newly synthesized DNA. Feeds were switched from normal feed to an HFD at the same day of BrdU administration to boost the proliferation of adipose precursors within adipose depots. After 1 week of administration, mice are sacrificed and SVFs are isolated, and stained with surface antibodies for Lin markers and PDGFRα. After fixation with successive incubation with 3.6% Formaldehyde (v/v) and ice-cold 70% (v/v) ethanol, cells are stained with anti-BrdU-FITC antibody, followed by the incubation of DAPI for 30 min at RT. The processed samples are analyzed with flow cytometry (BD LSR Fortessa). Cells that were not incubated with antibody were used as a negative control to determine background fluorescence levels and BrdU positive area was set based on the signals from positive control cells provided in the kit.

Hydroxyproline assays—Hydroxyproline content in adipose was assayed using the Hydroxyproline Colorimetric Assay kit (BioVision, K555) according to the manufacturer's protocol. Briefly, 100–150 mg of frozen adipose tissues were homogenized and incubated in 12 N HCL for 3 h at 120°C. Samples were reacted with Chloramine T reagent for 5 min at RT. OD560 measurements were made on a plate reader (SpectraMAX i3 Plate reader) at 25°C, and the data were calculated using a standard curve.

Author Manuscript Author Manuscript Author Manuscript Author Manuscript

Adipocyte size distribution and number analysis—The H&E images were captured using an AxioImager M1 microscope (Zeiss, Germany). Individual adipocyte area [μm^2] was measured using an automated software called Adiposoft.[75] To estimate the total number of cells in the fat pads, the fat pad volume (V_{fat_pad}) was divided by the average fat cell volume (V_{fat_cell}). The fat pad volume (V_{fat_pad}) was calculated by dividing the fat pad mass by the adipose density, which was determined to be 0.95 g/cm.[89] The density value was obtained through Monte Carlo simulations using adipose tissue derived from a mouse model.[89] The volume of the fat cells was calculated using the following formula.[90,91] ($V_{fat\_cell} = \frac{1}{6}\pi d^3$, where the mean diameter (d) was calculated as $2 \times \sqrt{mean\ cell\ area/\pi}$). To account for the variation in fat cell size, $\left(3\sigma^2 \times d + d^3\right)$ was used instead of d^3 to calculate the fat cell volume, where σ represents the standard deviation of the diameter.[91,92]

Immunofluorescence assay—Adipose tissues were fixed with neutral-buffered formalin and embedded in paraffin. Fixed tissues were permeabilized with PBS containing 0.1% Triton X-100 for 10 min and then incubated with anti-MAC2 antibodies in PBS containing 10% (v/v) FBS for 18 h at 4°C. The cover slide was washed and incubated with FITC-conjugated anti-rat IgG for 1 h. Staining was analyzed with a confocal LSM710 microscope (Carl Zeiss Microimaging Inc.).

RNA-seq library generation and analysis—RNA samples were extracted using the RNAqueous-Micro Kit (Cat# AM1931), and the quality of total RNA was assessed by the 2100 Bioanalyzer (Agilent). Libraries were prepared using the Poly(A) RNA Selection Kit V1.5. RNA-seq reads were aligned to the UCSC mm10 genome using Hisat2.[76] Gene expression levels were measured from feature counts using Htseq.[77] Differential-expression analysis was done using Deseq2,[78] and differentially expressed genes upon KO were selected by fold-change >1.25 & FDR <0.05. Enrichment analysis was performed using GSEApy[79] to generate enrichment terms and pathways from the KEGG 2019 Mouse. RNA-seq raw data is available in GEO (GSE214483).

WGBS analysis—Raw reads were quality and adapter trimmed using FastQC (v0.11.7) and TrimGalore (v0.6.1) prior to mapping to the *in-silico* bisulfite converted mouse genome (GRCm39) using Bismark (v0.18.1).[80] CpG methylation calls were extracted after alignment with Bismark as well. Differentially Methylation Region (DMR) was called by DSS (v2.45.0)[81] in R (v4.1.2) environment. Genomic regions with more than 5 CpGs in 200bp bins, and minimal methylation level differences (>20%, $p < 0.01$) were defined as DMRs. Functional enrichment analysis of DMRs was done using GREAT (v4.0.4)[82] by finding genes associated to DMRs. For transcription factor motif enrichment, HOMER (v4.11)[83] analysis was used for finding *de novo* motif enrichments of DMRs. The program findMotifs.pl with default parameters was used to find motifs on the DMRs. WGBS sequencing data is available in GEO (GSE214483).

Bone μCT analysis—Murine tibiae were harvested at necropsy, fixed in paraformaldehyde for 48+ hours, washed 3X with PBS, and stored in Sorensen phosphate buffer at 4°C. μCT analysis was performed as previously described.[93] Briefly, tibiae were

Author Manuscript Author Manuscript Author Manuscript Author Manuscript

placed in a 19-mm diameter specimen holder and scanned over the entire length of the tibiae using a μCT system (μCT100 Scanco Medical, Bassersdorf, Switzerland). The following scan settings were used: voxel size 12 μm, 70 kVp, 114 μA, 0.5 mm AL filter, and integration time 500ms. Density measurements were calibrated to the manufacturer's hydroxyapatite phantom. Analysis was performed using the manufacturer's evaluation software with a threshold of 180 for trabecular bone and 280 for cortical bone.

TG measurements in tissues—Frozen tissues (100 mg) were weighted and transferred into Eppendorf tubes. The tissues were digested with 1mL of alkali digested buffer (6.2% potassium hydroxide in EtOH solution) for O/N at 55°C. Digested tissues are centrifuged at 5,000 rpm for 5 min and supernatants are acquired. Then, 1.1 supernatants volume of 1M $MgCl_2$ was added. After 10 min of incubation on ice, samples were centrifuged at 5,000 rpm for 5 min and supernatants were acquired. TG levels were measured with a Serum Triglyceride Determination Kit (TR0100, Sigma) following the manufacturer's protocol. Briefly, 80 μL of free glycerol reagent was dispensed into a 96-well plate. Then, 1 μL of final supernatants were added and incubated for 15 min at RT. Finally, 20 μL of Lipase containing Triglyceride Reagent was added and incubated for 15 min at RT, followed by absorbance measurement at 540 nm.

QUANTIFICATION AND STATISTICAL ANALYSIS

Where appropriate, data are expressed as mean ± SEM. The data were statistically analyzed using unpaired Student's t-test and two-way ANOVA with Tukey's multiple comparisons test using GraphPad Prism version 8. The p values below 0.05 were considered statistically significant. *$p < 0.05$, **$p < 0.01$, ***$p < 0.001$. Replicate information is indicated in the figures.

Supplementary Material

Refer to Web version on PubMed Central for supplementary material.

ACKNOWLEDGMENTS

The authors thank Dr. Chao Wang (University of Chinese Academy of Sciences) for sharing the TET3-CD mutant construct. We thank Dr. Andreas Stahl (University of California, Berkeley) for shearing the pLN-U6-gRNA plasmid. We thank Dr. Michael Rehli (University Hospital Regensburg) for shearing the pCpGL3-Basic plasmid. This work was funded by R01 DK116008 (NIDDK) and P&F P30DK116074 (Stanford Diabetes Research Center) to S.K.

REFERENCES

1. Rosen ED, and Spiegelman BM (2006). Adipocytes as regulators of energy balance and glucose homeostasis. Nature 444, 847–853. 10.1038/nature05483. [PubMed: 17167472]
2. Reilly SM, and Saltiel AR (2017). Adapting to obesity with adipose tissue inflammation. Nat. Rev. Endocrinol. 13, 633–643. 10.1038/nrendo.2017.90. [PubMed: 28799554]
3. Scherer PE (2006). Adipose tissue: from lipid storage compartment to endocrine organ. Diabetes 55, 1537–1545. 10.2337/db06-0263. [PubMed: 16731815]
4. Wang F, Mullican SE, DiSpirito JR, Peed LC, and Lazar MA(2013). Lipoatrophy and severe metabolic disturbance in mice with fat-specific deletion of PPARgamma. Proc. Natl. Acad. Sci. USA 110, 18656–18661. 10.1073/pnas.1314863110. [PubMed: 24167256]

Author Manuscript Author Manuscript Author Manuscript Author Manuscript

5. He W, Barak Y, Hevener A, Olson P, Liao D, Le J, Nelson M, Ong E, Olefsky JM, and Evans RM (2003). Adipose-specific peroxisome proliferator-activated receptor gamma knockout causes insulin resistance in fat and liver but not in muscle. Proc. Natl. Acad. Sci. USA 100, 15712–15717. 10.1073/pnas.2536828100. [PubMed: 14660788]
6. Inagaki T, Sakai J, and Kajimura S (2016). Transcriptional and epigenetic control of brown and beige adipose cell fate and function. Nat. Rev. Mol. Cell Biol. 17, 480–495. 10.1038/nrm.2016.62. [PubMed: 27251423]
7. Jung BC, and Kang S (2021). Epigenetic regulation of inflammatory factors in adipose tissue. Biochim. Biophys. Acta. Mol. Cell Biol. Lipids 1866, 159019. 10.1016/j.bbalip.2021.159019.
8. Damal Villivalam S, You D, Kim J, Lim HW, Xiao H, Zushin PJH,Oguri Y, Amin P, and Kang S (2020). TET1 is a beige adipocyte-selective epigenetic suppressor of thermogenesis. Nat. Commun. 11, 4313. 10.1038/s41467-020-18054-y. [PubMed: 32855402]
9. You D, Nilsson E, Tenen DE, Lyubetskaya A, Lo JC, Jiang R, Deng J, Dawes BA, Vaag A, Ling C, et al. (2017). Dnmt3a is an epigenetic mediator of adipose insulin resistance. Elife 6, e30766. 10.7554/eLife.30766.
10. Jones PA (2012). Functions of DNA methylation: islands, start sites, genebodies and beyond. Nat. Rev. Genet. 13, 484–492. 10.1038/nrg3230. [PubMed: 22641018]
11. Luo C, Hajkova P, and Ecker JR (2018). Dynamic DNA methylation: In the right place at the right time. Science 361, 1336–1340. 10.1126/science.aat6806. [PubMed: 30262495]
12. Bian F, Ma X, Villivalam SD, You D, Choy LR, Paladugu A, Fung S, and Kang S (2018). TET2 facilitates PPARgamma agonist-mediated gene regulation and insulin sensitization in adipocytes. Metabolism 89, 39–47. 10.1016/j.metabol.2018.08.006. [PubMed: 30193945]
13. Park YJ, Lee S, Lim S, Nahmgoong H, Ji Y, Huh JY, Alfadda AA, Kim S, and Kim JB (2021). DNMT1 maintains metabolic fitness of adipocytes through acting as an epigenetic safeguard of mitochondrial dynamics. Proc. Natl. Acad. Sci. USA 118, e2021073118. 10.1073/pnas.2021073118.
14. Kim AY, Park YJ, Pan X, Shin KC, Kwak SH, Bassas AF, Sallam RM, Park KS, Alfadda AA, Xu A, and Kim JB (2015). Obesity-induced DNA hypermethylation of the adiponectin gene mediates insulin resistance. Nat. Commun. 6, 7585. 10.1038/ncomms8585. [PubMed: 26139044]
15. Fujiki K, Shinoda A, Kano F, Sato R, Shirahige K, and Murata M(2013). PPARgamma-induced PARylation promotes local DNA demethylation by production of 5-hydroxymethylcytosine. Nat. Commun. 4, 2262. 10.1038/ncomms3262. [PubMed: 23912449]
16. Li J, Zhang N, Huang X, Xu J, Fernandes JC, Dai K, and Zhang X(2013). Dexamethasone shifts bone marrow stromal cells from osteoblasts to adipocytes by C/EBPalpha promoter methylation. Cell Death Dis. 4, e832. 10.1038/cddis.2013.348. [PubMed: 24091675]
17. Yoo Y, Park JH, Weigel C, Liesenfeld DB, Weichenhan D, Plass C,Seo DG, Lindroth AM, and Park YJ (2017). TET-mediated hydroxymethylcytosine at the Ppargamma locus is required for initiation of adipogenic differentiation. Int. J. Obes. 41, 652–659. 10.1038/ijo.2017.8.
18. Matsumura Y, Nakaki R, Inagaki T, Yoshida A, Kano Y, Kimura H, Tanaka T, Tsutsumi S, Nakao M, Doi T, et al. (2015). H3K4/H3K9me3 Bivalent Chromatin Domains Targeted by Lineage-Specific DNA Methylation Pauses Adipocyte Differentiation. Mol. Cell 60, 584–596. 10.1016/j.molcel.2015.10.025. [PubMed: 26590716]
19. Kuroda M, Tominaga A, Nakagawa K, Nishiguchi M, Sebe M, Miyatake Y, Kitamura T, Tsutsumi R, Harada N, Nakaya Y, and Sakaue H (2016). DNA Methylation Suppresses Leptin Gene in 3T3-L1 Adipocytes. PLoS One 11, e0160532. 10.1371/journal.pone.0160532.
20. Yokomori N, Tawata M, and Onaya T (1999). DNA demethylation during the differentiation of 3T3-L1 cells affects the expression of the mouse GLUT4 gene. Diabetes 48, 685–690. 10.2337/diabetes.48.4.685. [PubMed: 10102682]
21. Dubois-Chevalier J, Oger F, Dehondt H, Firmin FF, Gheeraert C, Staels B, Lefebvre P, and Eeckhoute J (2014). A dynamic CTCF chromatin binding landscape promotes DNA hydroxymethylation and transcriptional induction of adipocyte differentiation. Nucleic Acids Res. 42, 10943–10959. 10.1093/nar/gku780. [PubMed: 25183525]

Author Manuscript Author Manuscript Author Manuscript Author Manuscript

22. Yu P, Ji L, Lee KJ, Yu M, He C, Ambati S, McKinney EC, Jackson C, Baile CA, Schmitz RJ, and Meagher RB (2016). Subsets of Visceral Adipose Tissue Nuclei with Distinct Levels of 5-Hydroxymethylcytosine. PLoS One 11, e0154949. 10.1371/journal.pone.0154949.

23. Berry R, and Rodeheffer MS (2013). Characterization of the adipocyte cellular lineage in vivo. Nat. Cell Biol. 15, 302–308. 10.1038/ncb2696. [PubMed: 23434825]

24. Cattaneo P, Mukherjee D, Spinozzi S, Zhang L, Larcher V, Stallcup WB, Kataoka H, Chen J, Dimmeler S, Evans SM, and Guimarães-Camboa N (2020). Parallel Lineage-Tracing Studies Establish Fibroblasts as the Prevailing In Vivo Adipocyte Progenitor. Cell Rep. 30, 571–582.e2. 10.1016/j.celrep.2019.12.046. [PubMed: 31940497]

25. Lee YH, Petkova AP, Mottillo EP, and Granneman JG (2012). In vivo identification of bipotential adipocyte progenitors recruited by beta3-adrenoceptor activation and high-fat feeding. Cell Metabol. 15, 480–491. 10.1016/j.cmet.2012.03.009.

26. Rivera-Gonzalez GC, Shook BA, Andrae J, Holtrup B, Bollag K, Betsholtz C, Rodeheffer MS, and Horsley V (2016). Skin Adipocyte Stem Cell Self-Renewal Is Regulated by a PDGFA/AKT-Signaling Axis. Cell Stem Cell 19, 738–751. 10.1016/j.stem.2016.09.002. [PubMed: 27746098]

27. Emont MP, Jacobs C, Essene AL, Pant D, Tenen D, Colleluori G, Di Vincenzo A, Jørgensen AM, Dashti H, Stefek A, et al. (2022). A single-cell atlas of human and mouse white adipose tissue. Nature 603, 926–933. 10.1038/s41586-022-04518-2. [PubMed: 35296864]

28. Hotamisligil GS (2017). Inflammation, metaflammation and immunometabolic disorders. Nature 542, 177–185. 10.1038/nature21363. [PubMed: 28179656]

29. Vishvanath L, and Gupta RK (2019). Contribution of adipogenesis to healthy adipose tissue expansion in obesity. J. Clin. Invest. 129, 4022–4031. 10.1172/JCI129191. [PubMed: 31573549]

30. Cawthorn WP, Scheller EL, Learman BS, Parlee SD, Simon BR, Mori H, Ning X, Bree AJ, Schell B, Broome DT, et al. (2014). Bone marrow adipose tissue is an endocrine organ that contributes to increased circulating adiponectin during caloric restriction. Cell Metabol. 20, 368–375. 10.1016/j.cmet.2014.06.003.

31. Jeffery E, Wing A, Holtrup B, Sebo Z, Kaplan JL, Saavedra-Peña R, Church CD, Colman L, Berry R, and Rodeheffer MS (2016). The Adipose Tissue Microenvironment Regulates Depot-Specific Adipogenesis in Obesity. Cell Metabol. 24, 142–150. 10.1016/j.cmet.2016.05.012.

32. Palmer BF, and Clegg DJ (2015). The sexual dimorphism of obesity. Mol. Cell. Endocrinol. 402, 113–119. 10.1016/j.mce.2014.11.029. [PubMed: 25578600]

33. Bilal M, Nawaz A, Kado T, Aslam MR, Igarashi Y, Nishimura A, Watanabe Y, Kuwano T, Liu J, Miwa H, et al. (2021). Fate of adipocyte progenitors during adipogenesis in mice fed a high-fat diet. Mol. Metabol. 54, 101328. 10.1016/j.molmet.2021.101328.

34. Lio CW, Zhang J, Gonzá lez-Avalos E, Hogan PG, Chang X, and Rao A (2016). Tet2 and Tet3 cooperate with B-lineage transcription factors to regulate DNA modification and chromatin accessibility. Elife 5, e18290. 10.7554/eLife.18290.

35. Sun K, Kusminski CM, and Scherer PE (2011). Adipose tissue remodeling and obesity. J. Clin. Invest. 121, 2094–2101. 10.1172/JCI45887. [PubMed: 21633177]

36. Lorenzo P, Neame P, Sommarin Y, and Heinegård D (1998). Cloning and deduced amino acid sequence of a novel cartilage protein (CILP) identifies a proform including a nucleotide pyrophosphohydrolase. J. Biol. Chem. 273, 23469–23475. 10.1074/jbc.273.36.23469. [PubMed: 9722584]

37. Wang Z, Kim JH, Higashino K, Kim SS, Wang S, Seki S, Hutton WC, and Yoon ST (2012). Cartilage intermediate layer protein (CILP) regulation in intervertebral discs. The effect of age, degeneration, and bone morphogenetic protein-2 Spine (Phila Pa 1976) 37, E203–E208. 10.1097/BRS.0b013e31822dcf47. [PubMed: 21857406]

38. van Nieuwenhoven FA, Munts C, Op't Veld RC, González A, Díez J, Heymans S, Schroen B, and van Bilsen M (2017). Cartilage intermediate layer protein 1 (CILP1): A novel mediator of cardiac extracellular matrix remodelling. Sci. Rep. 7, 16042. 10.1038/s41598-017-16201-y. [PubMed: 29167509]

39. Zhang CL, Zhao Q, Liang H, Qiao X, Wang JY, Wu D, Wu LL, and Li L (2018). Cartilage intermediate layer protein-1 alleviates pressure overload-induced cardiac fibrosis via interfering

Author Manuscript Author Manuscript Author Manuscript Author Manuscript

TGF-beta1 signaling. J. Mol. Cell. Cardiol. 116, 135–144. 10.1016/j.yjmcc.2018.02.006. [PubMed: 29438665]

40. McLellan MA, Skelly DA, Dona MSI, Squiers GT, Farrugia GE, Gaynor TL, Cohen CD, Pandey R, Diep H, Vinh A, et al. (2020). High-Resolution Transcriptomic Profiling of the Heart During Chronic Stress Reveals Cellular Drivers of Cardiac Fibrosis and Hypertrophy. Circulation 142, 1448–1463. 10.1161/CIRCULATIONAHA.119.045115. [PubMed: 32795101]
41. Huang Z, Zhang Z, Moazzami Z, Heck R, Hu P, Nanda H, Ren K, Sun Z, Bartolomucci A, Gao Y, et al. (2022). Brown adipose tissue involution associated with progressive restriction in progenitor competence. Cell Rep. 39, 110575. 10.1016/j.celrep.2022.110575.
42. Zachara M, Rainer PY, Hashimi H, Russeil JM, Alpern D, Ferrero R, Litovchenko M, and Deplancke B (2022). Mammalian adipogenesis regulator (Areg) cells use retinoic acid signalling to be non- and anti-adipogenic in age-dependent manner. EMBO J. 41, e108206. 10.15252/embj.2021108206.
43. Pastor WA, Aravind L, and Rao A (2013). TETonic shift: biological rolesof TET proteins in DNA demethylation and transcription. Nat. Rev. Mol. Cell Biol. 14, 341–356. 10.1038/nrm3589. [PubMed: 23698584]
44. Xue S, Liu C, Sun X, Li W, Zhang C, Zhou X, Lu Y, Xiao J, Li C,Xu X, et al. (2016). TET3 Inhibits Type I IFN Production Independent of DNA Demethylation. Cell Rep. 16, 1096–1105. 10.1016/j.celrep.2016.06.068. [PubMed: 27425624]
45. Li S, and Tollefsbol TO (2021). DNA methylation methods: Global DNA methylation and methylomic analyses. Methods 187, 28–43. 10.1016/j.ymeth.2020.10.002. [PubMed: 33039572]
46. Klug M, and Rehli M (2006). Functional analysis of promoter CpG methylation using a CpG-free luciferase reporter vector. Epigenetics 1, 127–130. 10.4161/epi.1.3.3327. [PubMed: 17965610]
47. Ma L, Tang Q, Gao X, Lee J, Lei R, Suzuki M, Zheng D, Ito K, Frenette PS, and Dawlaty MM (2022). Tet-mediated DNA demethylation regulates specification of hematopoietic stem and progenitor cells during mammalian embryogenesis. Sci. Adv. 8, eabm3470. 10.1126/sciadv.abm3470.
48. Fang S, Li J, Xiao Y, Lee M, Guo L, Han W, Li T, Hill MC, Hong T, Mo W, et al. (2019). Tet inactivation disrupts YY1 binding and long-range chromatin interactions during embryonic heart development. Nat. Commun. 10, 4297. 10.1038/s41467-019-12325-z. [PubMed: 31541101]
49. Hiraike Y, Waki H, Miyake K, Wada T, Oguchi M, Saito K, Tsutsumi S, Aburatani H, Yamauchi T, and Kadowaki T (2020). NFIA differentially controls adipogenic and myogenic gene program through distinct pathways to ensure brown and beige adipocyte differentiation. PLoS Genet. 16, e1009044. 10.1371/journal.pgen.1009044.
50. Hiraike Y, Waki H, Yu J, Nakamura M, Miyake K, Nagano G, Nakaki R, Suzuki K, Kobayashi H, Yamamoto S, et al. (2017). NFIA co-localizes with PPARgamma and transcriptionally controls the brown fat gene program. Nat. Cell Biol. 19, 1081–1092. 10.1038/ncb3590. [PubMed: 28812581]
51. Waki H, Nakamura M, Yamauchi T, Wakabayashi K.i., Yu J, Hirose-Yotsuya L, Take K, Sun W, Iwabu M, Okada-Iwabu M, et al. (2011). Global mapping of cell type-specific open chromatin by FAIRE-seq reveals the regulatory role of the NFI family in adipocyte differentiation. PLoS Genet. 7, e1002311. 10.1371/journal.pgen.1002311.
52. Darlington GJ, Ross SE, and MacDougald OA (1998). The role of C/EBP genes in adipocyte differentiation. J. Biol. Chem. 273, 30057–30060. 10.1074/jbc.273.46.30057. [PubMed: 9804754]
53. Park J, Lee DH, Ham S, Oh J, Noh JR, Lee YK, Park YJ, Lee G,Han SM, Han JS, et al. (2022). Targeted erasure of DNA methylation by TET3 drives adipogenic reprogramming and differentiation. Nat. Metab. 4, 918–931. 10.1038/s42255-022-00597-7. [PubMed: 35788760]
54. Siersbæk R, Nielsen R, John S, Sung MH, Baek S, Loft A, Hager GL, and Mandrup S (2011). Extensive chromatin remodelling and establishment of transcription factor ‘hotspots’ during early adipogenesis. EMBO J. 30, 1459–1472. 10.1038/emboj.2011.65. [PubMed: 21427703]
55. Werman A, Hollenberg A, Solanes G, Bjorbaek C, Vidal-Puig AJ,and Flier JS (1997). Ligand-independent activation domain in the N terminus of peroxisome proliferator-activated receptor gamma (PPARgamma). Differential activity of PPARgamma1 and −2 isoforms and influence of insulin. J. Biol. Chem. 272, 20230–20235. 10.1074/jbc.272.32.20230. [PubMed: 9242701]

Author Manuscript Author Manuscript Author Manuscript Author Manuscript

56. Ricote M, Li AC, Willson TM, Kelly CJ, and Glass CK (1998). The peroxisome proliferator-activated receptor-gamma is a negative regulator of macrophage activation. Nature 391, 79–82. 10.1038/34178. [PubMed: 9422508]
57. Verma N, Pan H, Doré LC, Shukla A, Li QV, Pelham-Webb B, Teijeiro V, González F, Krivtsov A, Chang CJ, et al. (2018). TET proteins safeguard bivalent promoters from de novo methylation in human embryonic stem cells. Nat. Genet. 50, 83–95. 10.1038/s41588-017-0002-y. [PubMed: 29203910]
58. Kim S, Huang LW, Snow KJ, Ablamunits V, Hasham MG, Young TH, Paulk AC, Richardson JE, Affourtit JP, Shalom-Barak T, et al. (2007). A mouse model of conditional lipodystrophy. Proc. Natl. Acad. Sci. USA 104, 16627–16632. 10.1073/pnas.0707797104. [PubMed: 17921248]
59. Pajvani UB, Trujillo ME, Combs TP, Iyengar P, Jelicks L, Roth KA, Kitsis RN, and Scherer PE (2005). Fat apoptosis through targeted activation of caspase 8: a new mouse model of inducible and reversible lipoatrophy. Nat. Med. 11, 797–803. 10.1038/nm1262. [PubMed: 15965483]
60. Péterfy M, Phan J, Xu P, and Reue K (2001). Lipodystrophy in the fld mouse results from mutation of a new gene encoding a nuclear protein, lipin. Nat. Genet. 27, 121–124. 10.1038/83685. [PubMed: 11138012]
61. Ross SR, Graves RA, and Spiegelman BM (1993). Targeted expression of a toxin gene to adipose tissue: transgenic mice resistant to obesity. Genes Dev. 7, 1318–1324. 10.1101/gad.7.7b.1318. [PubMed: 8330737]
62. Kubota N, Terauchi Y, Miki H, Tamemoto H, Yamauchi T, Komeda K, Satoh S, Nakano R, Ishii C, Sugiyama T, et al. (1999). PPAR gamma mediates high-fat diet-induced adipocyte hypertrophy and insulin resistance. Mol. Cell 4, 597–609. 10.1016/s1097-2765(00)80210-5. [PubMed: 10549291]
63. Hu W, Jiang C, Kim M, Xiao Y, Richter HJ, Guan D, Zhu K, Krusen BM, Roberts AN, Miller J, et al. (2022). Isoform-specific functions of PPARgamma in gene regulation and metabolism. Genes Dev. 36, 300–312. 10.1101/gad.349232.121. [PubMed: 35273075]
64. Spiegelman BM, and Ginty CA (1983). Fibronectin modulation of cell shape and lipogenic gene expression in 3T3-adipocytes. Cell 35, 657–666. 10.1016/0092-8674(83)90098-3. [PubMed: 6686086]
65. Pierleoni C, Verdenelli F, Castellucci M, and Cinti S (1998). Fibronectins and basal lamina molecules expression in human subcutaneous white adipose tissue. Eur. J. Histochem. 42, 183–188. [PubMed: 9857243]
66. Pope BD, Warren CR, Parker KK, and Cowan CA (2016). Microenvironmental Control of Adipocyte Fate and Function. Trends Cell Biol. 26, 745–755. 10.1016/j.tcb.2016.05.005. [PubMed: 27268909]
67. Henegar C, Tordjman J, Achard V, Lacasa D, Cremer I, Guerre-Millo M, Poitou C, Basdevant A, Stich V, Viguerie N, et al. (2008). Adipose tissue transcriptomic signature highlights the pathological relevance of extracellular matrix in human obesity. Genome Biol. 9, R14. 10.1186/gb-2008-9-1-r14. [PubMed: 18208606]
68. Williams AS, Kang L, and Wasserman DH (2015). The extracellular matrix and insulin resistance. Trends Endocrinol. Metabol. 26, 357–366. 10.1016/j.tem.2015.05.006.
69. Sun K, Tordjman J, Clément K, and Scherer PE (2013). Fibrosis and adipose tissue dysfunction. Cell Metabol. 18, 470–477. 10.1016/j.cmet.2013.06.016.
70. Ruiz-Ojeda FJ, Méndez-Gutié rrez A, Aguilera CM, and Plaza-Díaz J (2019). Extracellular Matrix Remodeling of Adipose Tissue in Obesity and Metabolic Diseases. Int. J. Mol. Sci. 20, 4888. 10.3390/ijms20194888. [PubMed: 31581657]
71. Pasarica M, Gowronska-Kozak B, Burk D, Remedios I, Hymel D, Gimble J, Ravussin E, Bray GA, and Smith SR (2009). Adipose tissue collagen VI in obesity. J. Clin. Endocrinol. Metab. 94, 5155–5162. 10.1210/jc.2009-0947. [PubMed: 19837927]
72. Khan T, Muise ES, Iyengar P, Wang ZV, Chandalia M, Abate N, Zhang BB, Bonaldo P, Chua S, and Scherer PE (2009). Metabolic dysregulation and adipose tissue fibrosis: role of collagen VI. Mol. Cell Biol. 29, 1575–1591. 10.1128/MCB.01300-08. [PubMed: 19114551]
73. Maquoi E, Munaut C, Colige A, Collen D, and Lijnen HR (2002). Modulation of adipose tissue expression of murine matrix metalloproteinases and their tissue inhibitors with obesity. Diabetes 51, 1093–1101. 10.2337/diabetes.51.4.1093. [PubMed: 11916931]

Author Manuscript Author Manuscript Author Manuscript Author Manuscript

74. Moffat J, Grueneberg DA, Yang X, Kim SY, Kloepfer AM, Hinkle G, Piqani B, Eisenhaure TM, Luo B, Grenier JK, et al. (2006). A lentiviral RNAi library for human and mouse genes applied to an arrayed viral high-content screen. Cell 124, 1283–1298. 10.1016/j.cell.2006.01.040. [PubMed: 16564017]

75. Galarraga M, Campión J, Muñoz-Barrutia A, Boqué N, Moreno H, Martínez JA, Milagro F, and Ortiz-de-Solórzano C (2012). Adiposoft: automated software for the analysis of white adipose tissue cellularity in histological sections. J. Lipid Res. 53, 2791–2796. 10.1194/jlr.D023788. [PubMed: 22993232]

76. Kim D, Langmead B, and Salzberg SL (2015). HISAT: a fast spliced aligner with low memory requirements. Nat. Methods 12, 357–360. 10.1038/nmeth.3317. [PubMed: 25751142]

77. Anders S, Pyl PT, and Huber W (2015). HTSeq–a Python framework to work with high-throughput sequencing data. Bioinformatics 31, 166–169. 10.1093/bioinformatics/btu638. [PubMed: 25260700]

78. Love MI, Huber W, and Anders S (2014). Moderated estimation of fold change and dispersion for RNA-seq data with DESeq2. Genome Biol. 15, 550. 10.1186/s13059-014-0550-8. [PubMed: 25516281]

79. Fang Z, Liu X, and Peltz G (2023). GSEApy: a comprehensive package for performing gene set enrichment analysis in Python. Bioinformatics 39, btac757. 10.1093/bioinformatics/btac757.

80. Krueger F, and Andrews SR (2011). Bismark: a flexible aligner and methylation caller for Bisulfite-Seq applications. Bioinformatics 27, 1571–1572. 10.1093/bioinformatics/btr167. [PubMed: 21493656]

81. Wu H, Xu T, Feng H, Chen L, Li B, Yao B, Qin Z, Jin P, and Conneely KN (2015). Detection of differentially methylated regions from whole-genome bisulfite sequencing data without replicates. Nucleic Acids Res. 43, e141. 10.1093/nar/gkv715. [PubMed: 26184873]

82. McLean CY, Bristor D, Hiller M, Clarke SL, Schaar BT, Lowe CB, Wenger AM, and Bejerano G (2010). GREAT improves functional interpretation of cis-regulatory regions. Nat. Biotechnol. 28, 495–501. 10.1038/nbt.1630. [PubMed: 20436461]

83. Heinz S, Benner C, Spann N, Bertolino E, Lin YC, Laslo P, Cheng JX, Murre C, Singh H, and Glass CK (2010). Simple combinations of lineage-determining transcription factors prime cis-regulatory elements required for macrophage and B cell identities. Mol. Cell 38, 576–589. 10.1016/j.molcel.2010.05.004. [PubMed: 20513432]

84. Andrews S (2010). FastQC: A Quality Control Tool for High Throughput Sequence Data. Available online at http://www.bioinformatics.babraham.ac.uk/projects/fastqc/.

85. Ko M, An J, Pastor WA, Koralov SB, Rajewsky K, and Rao A(2015). TET proteins and 5-methylcytosine oxidation in hematological cancers. Immunol. Rev. 263, 6–21. 10.1111/imr.12239. [PubMed: 25510268]

86. Virtue S, and Vidal-Puig A (2021). GTTs and ITTs in mice: simple tests, complex answers. Nat. Metab. 3, 883–886. 10.1038/s42255-021-00414-7. [PubMed: 34117483]

87. Wolever TM, and Jenkins DJ (1986). The use of the glycemic index in predicting the blood glucose response to mixed meals. Am. J. Clin. Nutr. 43, 167–172. 10.1093/ajcn/43.1.167. [PubMed: 3942088]

88. Levy JC, Matthews DR, and Hermans MP (1998). Correct homeostasis model assessment (HOMA) evaluation uses the computer program. Diabetes Care 21, 2191–2192. 10.2337/diacare.21.12.2191. [PubMed: 9839117]

89. Bitar A, Lisbona A, Thedrez P, Sai Maurel C, Le Forestier D, Barbet J, and Bardies M (2007). A voxel-based mouse for internal dose calculations using Monte Carlo simulations (MCNP). Phys. Med. Biol. 52, 1013–1025. 10.1088/0031-9155/52/4/010. [PubMed: 17264367]

90. Honecker J, Weidlich D, Heisz S, Lindgren CM, Karampinos DC, Claussnitzer M, and Hauner H (2021). A distribution-centered approach for analyzing human adipocyte size estimates and their association with obesity-related traits and mitochondrial function. Int. J. Obes. 45, 2108–2117. 10.1038/s41366-021-00883-6.

91. Sjöström L, Björntorp P, and Vrána J (1971). Microscopic fat cell size measurements on frozen-cut adipose tissue in comparison with automatic determinations of osmium-fixed fat cells. J. Lipid Res. 12, 521–530. [PubMed: 5098392]

Author Manuscript Author Manuscript Author Manuscript Author Manuscript

92. Arner P, Andersson DP, Thörne A, Wirén M, Hoffstedt J, Näslund E, Thorell A, and Rydén M (2013). Variations in the size of the major omentum are primarily determined by fat cell number. J. Clin. Endocrinol. Metab. 98, E897–E901. 10.1210/jc.2012-4106. [PubMed: 23543656]

93. Li Z, Bowers E, Zhu J, Yu H, Hardij J, Bagchi DP, Mori H, Lewis KT, Granger K, Schill RL, et al. (2022). Lipolysis of bone marrow adipocytes is required to fuel bone and the marrow niche during energy deficits. Elife 11, e78496. 10.7554/eLife.78496.

Author Manuscript Author Manuscript Author Manuscript Author Manuscript

Highlights

- TET3 is necessary for full adipogenesis *in vivo*
- TET3 is necessary for diet-induced unhealthy adipose expansion
- Reduced adipogenesis by the loss of TET3 in APCs leads to enhanced whole-body metabolism
- TET3 regulates a set of APC target genes by modulating their DNA methylation profile

Author Manuscript Author Manuscript Author Manuscript Author Manuscript

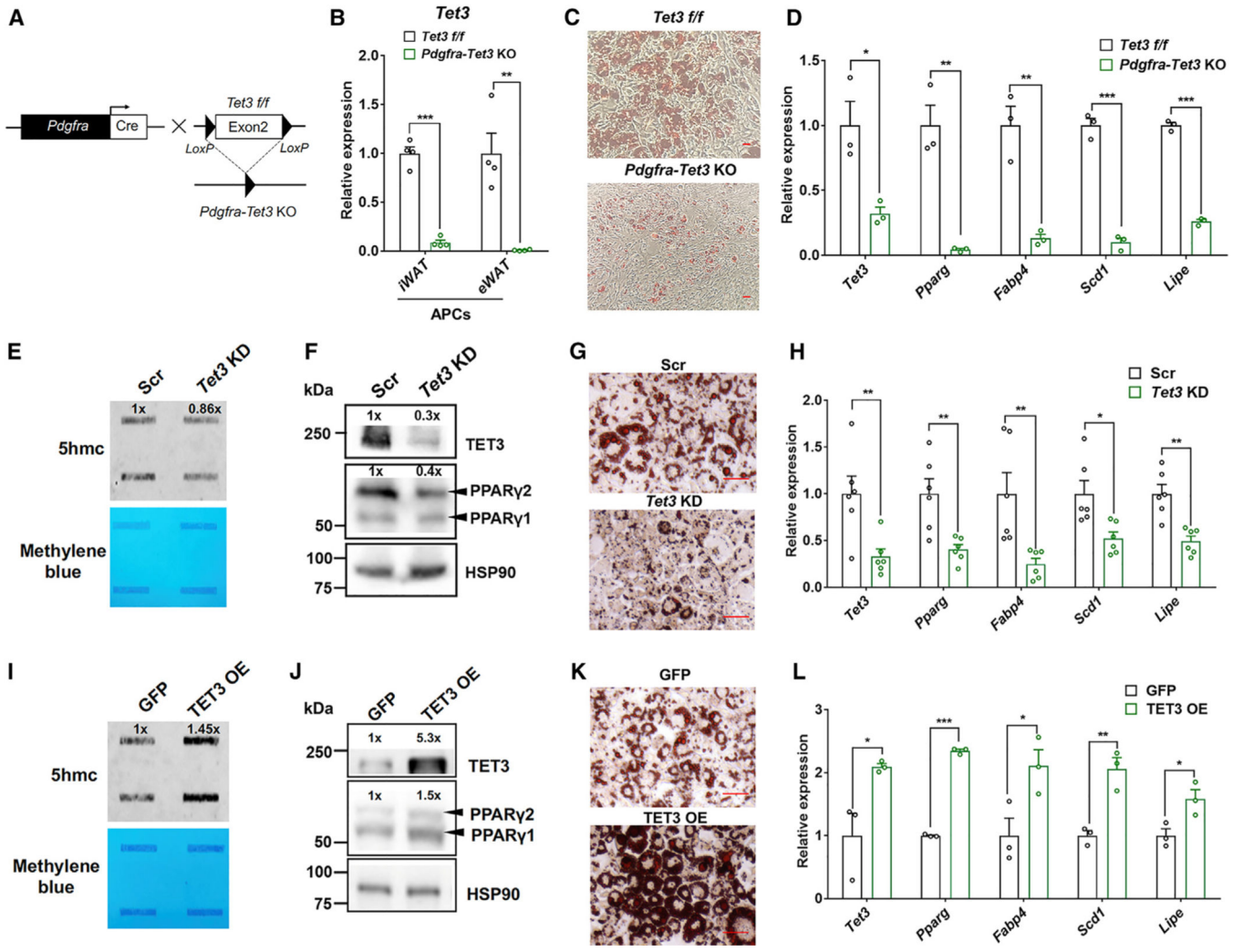

Figure 1. TET3 is necessary for full adipogenesis *in vitro* and *ex vivo*

(A) Cartoon of breeding strategy to generate APC-selective *Tet3* KO (*Pdgfra-Tet3* KO) mice.

(B) KD efficiency of *Tet3* in Lin$^-$/PDGFRα$^+$ APCs from iWAT of WT and KO mice (n = 4), determined using qPCR.

(C and D) Adipogenic potential was estimated by oil red O (ORO) staining (C) and mRNA expression analysis (D) in primary WT and *Tet3*-KO APCs at day 6 of adipogenesis (n = 3).

(E and I) Dot blot analysis showing global 5hmC levels in 3T3-L1 transduced with scramble (Scr), *shTet3* (*Tet3* KD), GFP, or TET3 (TET3 OE) plasmids. Methylene blue staining was used as a loading control.

(F–H and J–L) Protein analysis (F and J), ORO staining (G and K), and mRNA expression analysis (H and L) following adipogenic differentiation of cells from (E) and (I) (n = 6 for H; n = 3 for L).

Data are presented as mean ± standard error of the mean (SEM). The scale bars in (C), (G), and (K) represent 50 μm. *p < 0.05, **p < 0.01, ***p < 0.001 using two-tailed Student's t test (B, D, H, and L).

Author Manuscript Author Manuscript Author Manuscript Author Manuscript

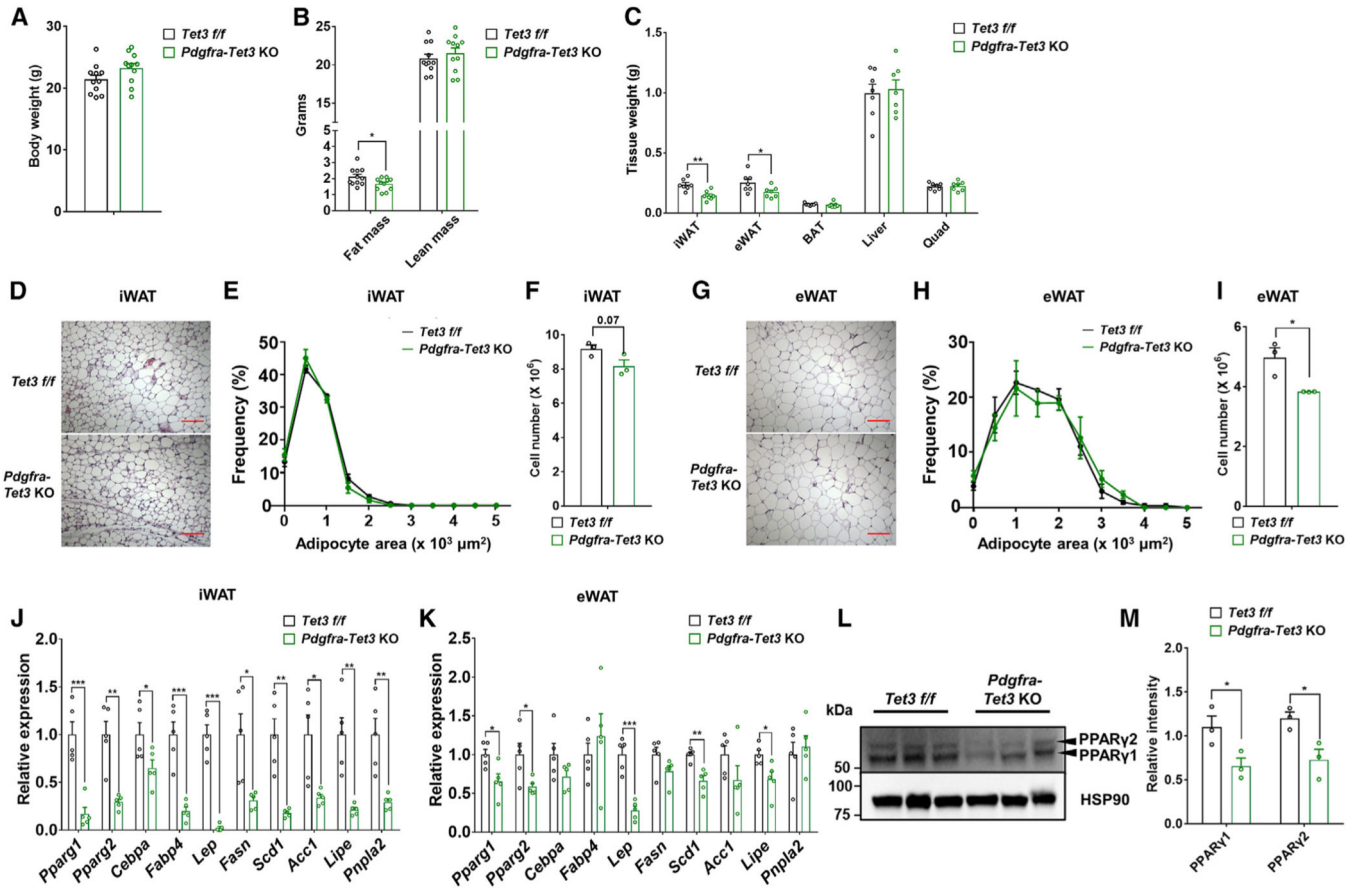

Figure 2. *Pdgfra-Tet3* KO male mice show reduced adiposity on a chow diet

(A–C) BW (A), body composition (B), and tissue weight (C) of 8-week-old WT and *Pdgfra-Tet3* KO male mice on a chow diet (n = 11 for A and B; n = 7 for C). Quad, quadriceps muscle.

(D–I) H&E staining (D and G), adipocyte size distribution (E and H), and total adipocyte number (F and I) of iWAT and eWAT from WT and *Pdgfra-Tet3* KO mice on a chow diet (n = 3 for E, F, H, and I). The scale bar represents 100 μm.

(J and K) Gene expression analysis in WAT from WT and *Pdgfra-Tet3* KO mice on a chow diet (n = 5).

(L and M) Immunoblotting analysis showing PPARγ protein levels in WAT from WT and *Pdgfra-Tet3* KO mice on a chow (n = 3).

Data are presented as mean ± SEM. *p < 0.05, **p < 0.01, ***p < 0.001 using two-tailed Student's t test (A–C, E, F, H–K, and M).

Author Manuscript Author Manuscript Author Manuscript Author Manuscript

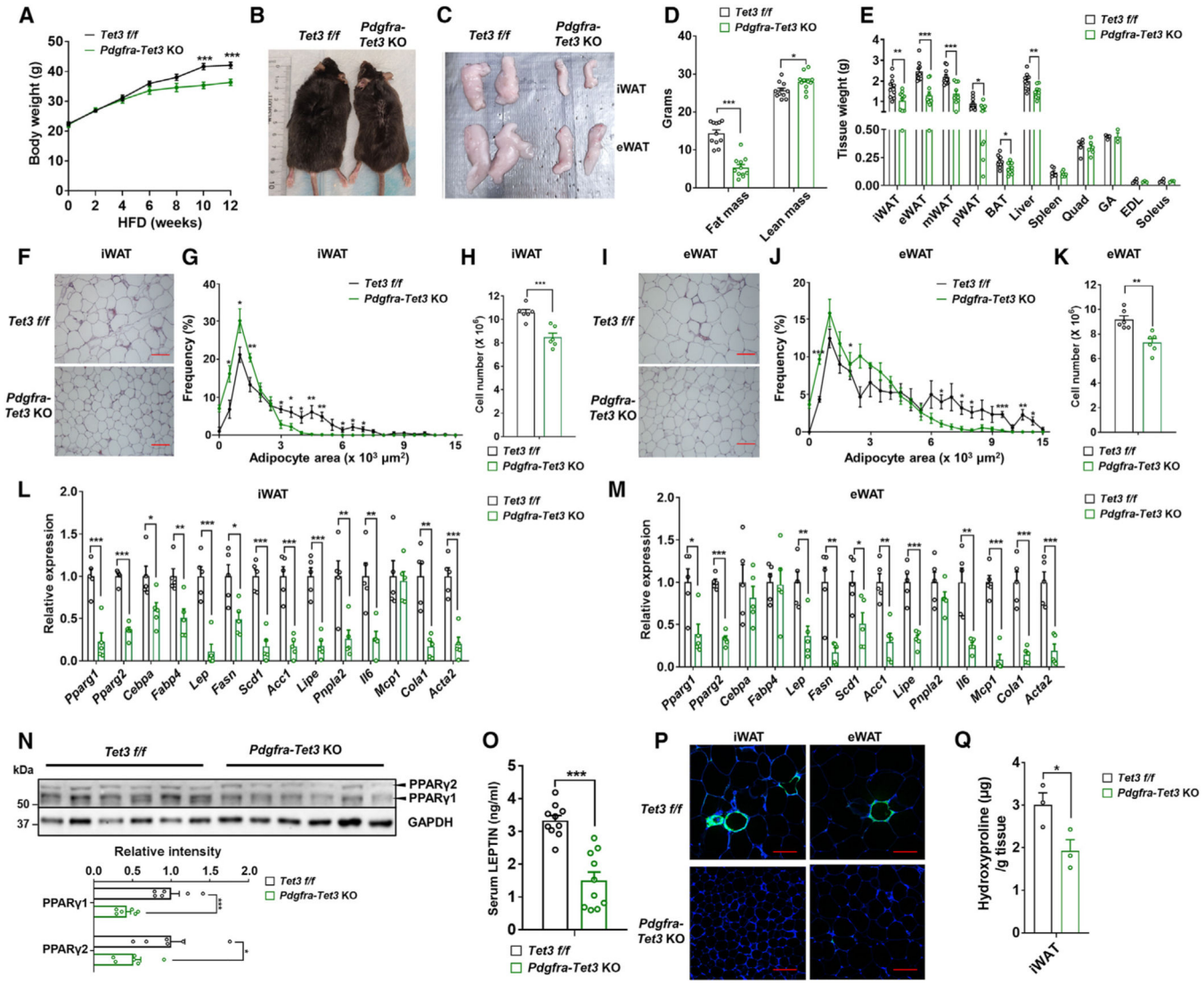

Figure 3. *Pdgfra-Tet3* KO male mice on an HFD are protected from unhealthy adipose expansion and remodelling

(A–E) BW (A), whole-body and WAT photographs (B and C), body composition (D), and adipose tissue weight (E) of WT and *Pdgfra-Tet3* KO male mice on an HFD. pWAT, perirenal WAT; mWAT, mesenteric WAT; GA, gastrocnemius; EDL, extensor digitorum longus (n = 11 for A and D; n = 10 for adipose tissues and liver; quad, spleen, GA, EDL, and soleus n = 4 [WT] or 3 [KO] in E).

(F–K) H&E staining (F and I), frequency distribution of adipocyte size (G and J), and total adipocyte number (H and K) of WATs from WT and *Pdgfra-Tet3* KO mice on an HFD (n = 6).

(L–N) mRNA expression analysis (L and M) and PPARγ protein levels and quantification (N) in WAT of WT and *Pdgfra-Tet3* KO mice on an HFD (n = 5 for L and M; n = 6 for N).

(O–Q) Serum leptin levels (O), immunofluorescence staining of Mac2 (P), and quantification of hydroxyproline (Q) in WAT from WT and KO mice on an HFD (n = 10 for O; n = 3 for Q). The scale bar represents 100 μm.

Author Manuscript Author Manuscript Author Manuscript Author Manuscript

Data are presented as mean ± SEM. *p < 0.05, **p < 0.01, ***p < 0.001 using two-tailed Student's t test (A, D, E, G, H, J–O, and Q).

Author Manuscript Author Manuscript Author Manuscript Author Manuscript

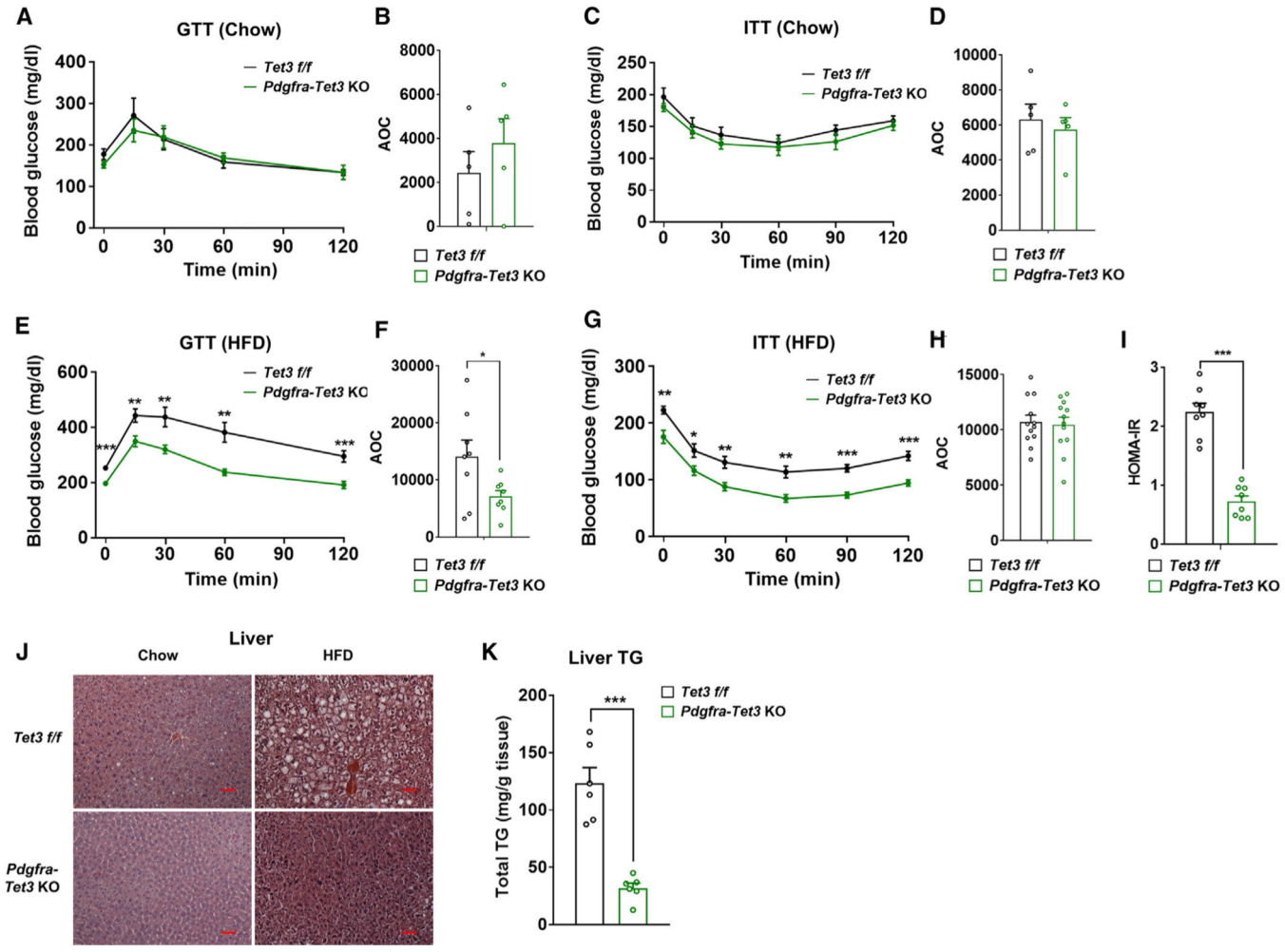

Figure 4. *Pdgfra-Tet3* KO male mice display improved whole-body metabolism on an HFD

(A–I) GTT (A, B, E, and F), ITT (C, D, G, and H), and HOMA-IR (I) from *Pdgfra-Tet3* KO and WT male mice reared on a chow at 8 weeks of age after being fed an HFD for 2 months (n = 5 mice for A–D; n = 8 mice for E, F, and I, n = 12 mice for G and H). AOC, area over the curve. Data are presented as mean ± SEM. *p < 0.05, using two-tailed Student's t test (A–G).

(J) H&E staining of liver sections of *Pdgfra-Tet3* KO and WT male mice on a chow and fed an HFD. The scale bar represents 50 μm

(K) Quantification of triglyceride (TG) in *Pdgfra-Tet3* KO and WT male mice fed an HFD (n = 6).

Data are presented as mean ± SEM. *p < 0.05, **p < 0.01, ***p < 0.001 using two-tailed Student's t test (A–I).

Author Manuscript Author Manuscript Author Manuscript Author Manuscript

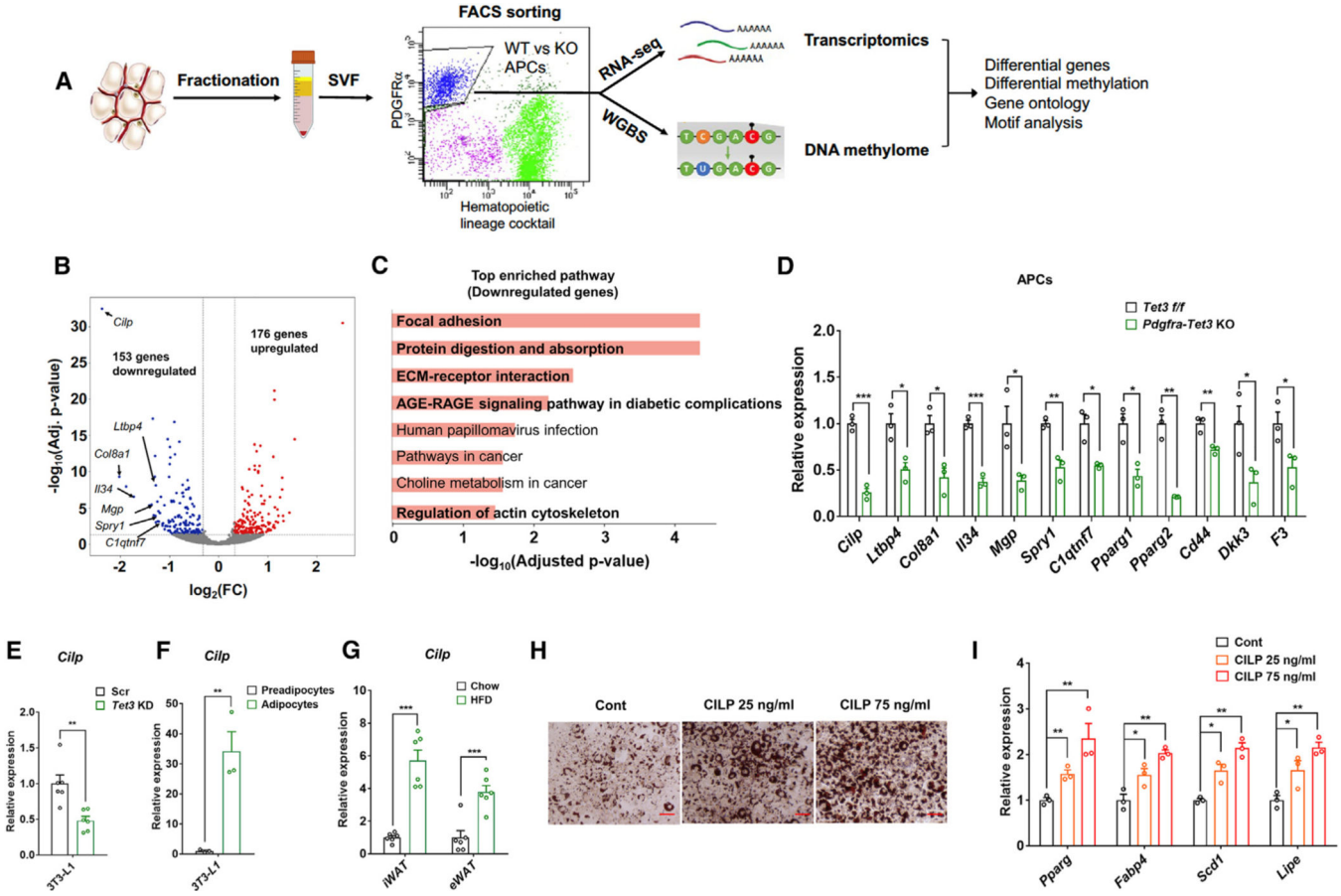

Figure 5. TET3 regulates the critical target genes involved in adipogenesis and remodeling in APCs

(A) Overall study design of transcriptomic and DNA methylome analysis of *Pdgfra-Tet3* KO vs. WT APCs.

(B) Volcano plot depicting up- and downregulated genes in *Pdgfra-Tet3* KO vs. WT iWAT APCs on an HFD.

(C) Top Kyoto Encyclopedia of Genes and Genomes (KEGG) pathways enriched in downregulated gene sets. ECM-related pathways are depicted in bold.

(D) qPCR validation of the downregulated genes in KO APCs (n = 3).

(E) mRNA expression of *Cilp* in confluent 3T3-L1 preadipocytes transduced with Scr or *shTet3* (n = 6).

(F and G) mRNA expression of *Cilp* during 3T3-L1 adipogenesis (F) and WATs from lean vs. obese WT C57BL/6J mice (G) (n = 3 for F; n = 6 for G).

(H and I) ORO staining (H) and gene expression analysis (I) in 3T3-L1 cells treated with vehicle (control [Cont]) and recombinant CILP (25 or 75 ng/mL) from adipogenic days 0–4. The scale bar represents 50 μm (n = 3 for I).

Data are presented as mean ± SEM. *p < 0.05, **p < 0.01, ***p < 0.001 using two-tailed Student's t test (D–G and I).

Author Manuscript Author Manuscript Author Manuscript Author Manuscript

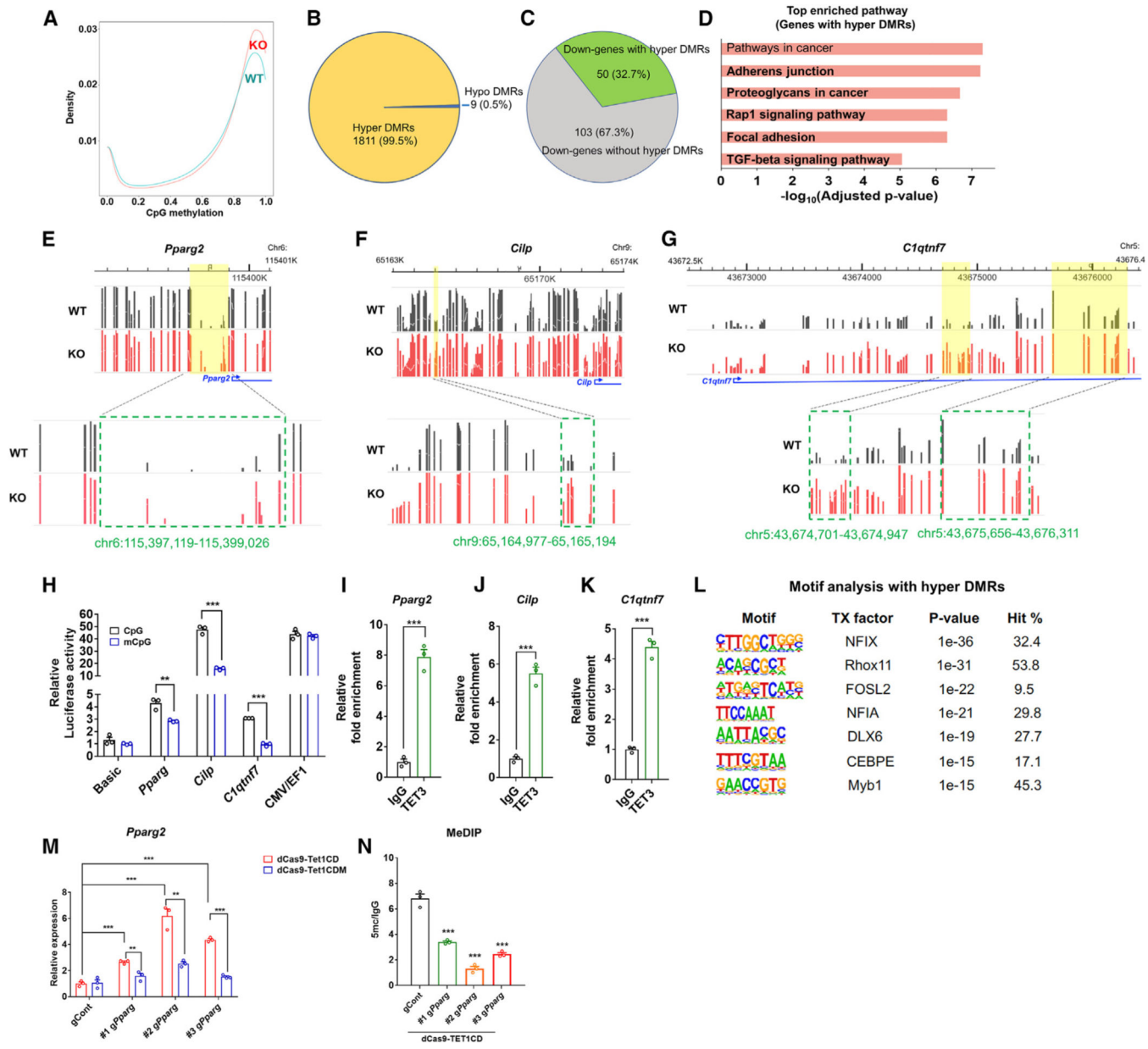

Figure 6. TET3 modifies the DNA methylation profile of key target genes in APCs

(A) Correlation map depicting relative CpG density and methylation levels between WT and *Tet3* KO APCs.

(B) Pie chart of hyper- and hypo-DMR counts in *Tet3* KO APCs.

(C) Pie chart of downregulated gene counts linked with hyper-DMRs in *Tet3* KO APCs.

(D) KEGG pathway most enriched in genes linked to hyper-DMRs in *Tet3* KO APCs. ECM-related pathways are depicted in bold.

(E–G) Snapshots of WGBS track showing hypermethylated regions (boxed region) near the TET3 target genes. The height of the gray and red bars represents the degree of CpG methylation in WT and *Tet3* KO APCs, respectively.

Author Manuscript Author Manuscript Author Manuscript Author Manuscript

(H) HEK-293T cells were transfected with methylated (mCpG) and unmethylated (CpG) versions of pCpGL reporter plasmids containing target regions with differential methylation or control sequences (basic and CMV/EF1 were used as a negative and positive controls, respectively). These cells were then assayed for luciferase reporter activity. The *C1qtnf7* DMR appeared on the left side of the track that was tested (n = 3).

(I–K) TET3 ChIP-qPCR analysis with WT iWAT at hypermethylated regions in *Tet3* KO APCs (n = 3).

(L) The overrepresented transcription factor motifs predicted by motif analysis using HOMER (v.4.11) on the hyper-DMRs in *Tet3* KO APCs.

(M and N) *Pparg2* mRNA expression (M) and 5mC enrichment at the *Pparg2* promoter (N) in 3T3-L1 preadipocytes expressing pINDUCER-dCas9-Tet1CD (dCas9-Tet1CD) or pINDUCER-dCas9-Tet1CDM (dCas9-Tet1CDM) compared with *Pparg* gRNAs (n = 3 for M and N).

Data are presented as mean ± SEM. **p < 0.01, ***p < 0.001 using two-tailed Student's t test (H–K, M, and N).

Author Manuscript Author Manuscript Author Manuscript Author Manuscript

KEY RESOURCES TABLE

REAGENT or RESOURCE	SOURCE	IDENTIFIER
Antibodies		
HSP-90	Cell Signaling	Cat# 4874; RRID:AB_2121214
GAPDH	Cell Signaling	Cat# 2118; RRID:AB_561053
Mouse (G3A1) mAb IgG1	Cell Signaling	Cat# 5415; RRID:AB_10829607
FLAG	Sigma	Cat# F3165; RRID:AB_259529
PDGFRα-PE	Invitrogen	Cat# 12–1401-81; AB_657615
CD45-APC	BD Biosciences	Cat# 561018; RRID:AB_10584326
CD31-APC	BD Biosciences	Cat# 561814; RRID:AB_10893351
TER119-APC	BD Biosciences	Cat# 561033; RRID:AB_10584336
5mc	Abcam	Cat# ab10805; RRID:AB_442823
5hmc	Active Motif	Cat# 39769; RRID:AB_10013602
PPARγ	Santa Cruz	Cat# sc-7273; RRID:AB_628115
MAC-2	Cedarlane Labs	Cat# CL8942AP; RRID:AB_10060357
TET3	Millipore	Cat# abe383
Chemicals, peptides, and recombinant proteins		
Insulin	Sigma	I5500
Dexamethasone	Sigma	D2915
isobutylmethylxanthine	Sigma	I5879
Puromycin	Sigma	P8833
Oil Red O	Sigma	O0625–100G
Methylene blue	Ricca Chemical	4880–100
Collagenase type 2	Fisher scientific	NC9693955
Recombinant CILP protein	Abcam	182802
TRI Reagent Solution	Invitrogen	AM9738
Dynabeads Protein G	Invitrogen	10004D
Dynabeads anti-mouse IgG	Fisher scientific	11–201-D
Protein assay dye reagent	Bio-Rad	5000006
BSA	Sigma	A7906
Lipofectamine 3000	Invitrogen	L3000–015
Critical commercial assays		
High-Capacity cDNA Reverse Transcription Kit	Applied Biosystems	4368813
SYBR green qPCR master mix	Bioneer	K-6251
mouse leptin ELISA Kit	Crystal Chem	90030
ultrasensitive mouse Insulin ELISA kit	Crystal Chem	90080
DNeasy Blood & Tissue kit	Qiagen	69504
APO-BrdU Fragmentation Assay Kit	BioVision	K401
RNAqueous®-Micro Kit	Invitrogen	AM1931

Author Manuscript Author Manuscript Author Manuscript Author Manuscript

REAGENT or RESOURCE	SOURCE	IDENTIFIER
ECL Assay Kit	PerkinElmer	NEL104001EA
Dual-Luciferase Reporter Assay System	Promega	E1980
Hydroxyproline Colorimetric Assay kit	BioVision	K555
Serum Triglyceride Determination Kit	Sigma	TR0100
Deposited data		
Whole genome bisulfite sequencing (WGBS) and RNA-sequencing of preadipocytes from iWAT	N/A	GSE214483
Experimental models: Cell lines		
3T3-L1	ATCC	CL-173
HEK293T	ATCC	CRL-3216
Experimental models: Organisms/strains		
Mouse: C57BL/6J	Jackson Laboratory	000664
Mouse: *Pdgfra-Tet3* KO	Dr. Anjana Rao and Jackson Laboratory	N/A
Oligonucleotides		
qPCR primer sequences	Integrated DNA technologies	Table S2
gRNA	Integrated DNA technologies	Table S2
ChIP-qPCR	Integrated DNA technologies	Table S2
MeDIP	Integrated DNA technologies	Table S2
Recombinant DNA		
pM2DG	gift from Dr. Didier Trono	Addgene, #12259
psPAX2	gift from Dr. Didier Trono	Addgene, #12260
pCDH-CMV-MCS-EF1	System Biosciences	CD510B-1
pLKO.1	gift from Dr. David Root[74]	Addgene, #10878
pLN-U6-gRNA	Dr. Andreas Stahl	N/A
pCpGL3-Basic	Dr. Michael Rehli	N/A
Software and algorithms		
QuantStudio 5	Applied Biosystems	A34322
iBright™ CL1500 Imaging System	Invitrogen	A44114
ImageJ	National Institutes of Health	https://imagej.nih.gov/ij/
Adiposoft[75]	Galarraga et al.[75]	https://drive.google.com/file/d/1TjfoogPQK2NB4VRpZxVn-BgcziCqrS8S/view
Hisat2[76]	Kim et al.[76]	https://github.com/DaehwanKimLab/hisat2
Htseq[77]	Anders et al.[77]	https://github.com/simon-anders/htseq
Deseq2[78]	Love et al.[78]	https://github.com/thelovelab/DESeq2
GSEApy[79]	Fang et al.[79]	https://github.com/zqfang/GSEApy/tree/v0.9.18
Bismark[80]	Krueger et al.[80]	https://github.com/FelixKrueger/Bismark

Author Manuscript

Author Manuscript

Author Manuscript

Author Manuscript

REAGENT or RESOURCE	SOURCE	IDENTIFIER
DSS[81]	Wu et al.[81]	https://github.com/haowulab/DSS/
GREAT[82]	McLean et al.[82]	http://great.stanford.edu/public/html/
Homer[83]	Heinz, S. et al.[83]	http://homer.ucsd.edu/homer/
FastQC	Andrews, S.[84]	https://github.com/s-andrews/FastQC
TrimGalore	Altos Labs	https://github.com/FelixKrueger/TrimGalore
GraphPad Prism	GraphPad	https://www.graphpad.com/
Other		
High fat diet	Research Diets	D12331i